DEVELOPMENT OF IN-VITRO AND IN-VIVO DEVICES TO STUDY THE MECHANOBIOLOGY OF LIGAMENT HEALING

by

John Bayard Everingham

A thesis

submitted in partial fulfillment

of the requirements for the degree of

Master of Science in Mechanical Engineering

Boise State University

December 2017

BOISE STATE UNIVERSITY GRADUATE COLLEGE

DEFENSE COMMITTEE AND FINAL READING APPROVALS

of the thesis submitted by

John Bayard Everingham

Thesis Title: Development of In-Vitro and In-Vivo Devices to Study the Mechanobiology of Ligament Healing

Date of Final Oral Examination: 9 November 2017

The following individuals read and discussed the thesis submitted by student John Bayard Everingham, and they evaluated his presentation and response to questions during the final oral examination. They found that the student passed the final oral examination.

Trevor Lujan, Ph.D.	Chair, Supervisory Committee
Gunes Uzer, Ph.D.	Member, Supervisory Committee
Julia Thom Oxford, Ph.D.	Member, Supervisory Committee
John F. Gardner, Ph.D.	Member, Supervisory Committee

The final reading approval of the thesis was granted by Trevor Lujan, Ph. D., Chair of the Supervisory Committee. The thesis was approved by the Graduate College.

DEDICATON

Dedicated to my supportive father, John M. Everingham

ACKNOWLEDGEMENTS

Research reported in this publication was supported by NIGMS under Grant Nos. P20GM109095 and P20GM103408. We also acknowledge support from the American Recover & Reinvestment Act, Grant No. 1C06RR020533; the Biomolecular Research Center at Boise State with funding from the NSF, Grants No. 0619793 and 0923535; the MJ Murdock Charitable Trust; and the Idaho State Board of Education.

I would like to thank Dr. Lujan for his mentorship and guidance throughout my studies at Boise State. I would like to extend thanks to Phil Boysen and Griffith Allen for helping me design and machine many of the components in this work. I would also like to thank Stephanie Tuft and Conner Patricelli for their assistance in all of the cell culture. I would like to thank Pete Martin and Abdullah Ahmad for their direct contributions on this work. I would like to thank all my coworkers in the Northwest Tissue Mechanics Lab for creating a productive and fun environment that made this work possible. Lastly, I would like to thank Jillian Helms for her daily love and support through my entire graduate degree.

ABSTRACT

Ligament injuries are the most common sports injury in the United States. The current clinical practice for treating ligament injuries leaves many patients with significant pain and joint laxity for years following the initial injury. Controlled mechanical stimulation of the tissue after injury is necessary for robust healing, but the optimal mechanical environment for ligament healing is not fully understood. Alternative therapies, such as instrument assisted soft tissue mobilization (IASTM), offer a form of mechanical stimulation that is non-invasive and has shown promising clinical outcomes but the optimal dosage for IASTM treatments is unknown. The objective of this study was to develop in-vitro and in-vivo experimental devices that can help determine the specific mechanical loads that strengthen and accelerate ligament healing.

Two devices were developed. The in-vitro device is a novel multi-axis mechanical stimulation bioreactor that can accurately apply tensile and combined tensile/compressive stress states to 3D fibroblast seeded tissue constructs. The bioreactor consists of two independently controlled actuators, one tensile, one compressive, a tablet computer, and data acquisition hardware. The bioreactor was validated using gelatin constructs to simultaneously apply cyclic forces from 0 – 0.2N with an accuracy of approximately 0.01N, and a high degree of repeatability. The in-vivo device is a hand-held device to control the frequency and magnitude of applied force during IASTM treatments on rats after ligament transection. The device consists of a force sensor, tablet computer, and custom software to guide the application of user-specified loading parameters during

IASTM treatments. The device accuracy was measured by applying a combination of force and stroke frequencies to rigid foam and was experimentally validated over a 3-week animal experiment. The device was demonstrated to apply forces between 0 – 5N at frequencies from 0 – 1Hz with a high degree of accuracy and repeatability.

The devices validated in this study provide a framework for future studies. The in-vitro device can provide insight into the mechanobiological effects of different loading configurations on fibroblast seeded constructs, including the simultaneous application of tensile and compressive loading, which is similar to IASTM treatment. The in-vivo device will be used to perform animal studies that can assess the effects of varying applied force and frequency parameters during IASTM treatments.

TABLE OF CONTENTS

DEDICATON iv

ACKNOWLEDGEMENTS v

ABSTRACT vi

LIST OF TABLES xi

LIST OF FIGURES xii

NOMENCLATURE xv

CHAPTER ONE: INTRODUCTION 1

1.1 Motivation 1

1.2 Research Goal 2

CHAPTER TWO: BACKGROUND 4

2.1 Ligament 4

2.1.1 Ligament Structure and Function 4

2.1.2 Ligament Wound Healing 5

2.1.3 Standard of Care 6

2.2 Instrument Assisted Soft Tissue Mobilization 7

2.2.1 Origins 7

2.2.2 Practical Application 8

2.2.3 Clinical and Biological Effects 9

2.2.4 Mechanisms 9

2.3 Mechanobiology 10

2.3.1 Mechanotranduction 10

2.3.2 In –Vitro Experimental Models 11

2.3.3 In-Vivo IASTM Experimental Models 12

CHAPTER THREE: MULTI-AXIS MECHANICAL STIMULATION BIOREACTOR FOR STIMULATION OF 3D CELLULAR CONSTRUCTS 15

3.1 Introduction 15

3.1.1 Mechanical Stimulation of Fibroblasts 15

3.1.2 Quantifying Mechanical Stimuli 16

3.1.3 Deviatoric vs. Dilatational 16

3.2 Methods 20

3.2.1 Bioreactor Design Criteria 20

3.2.2 Bioreactor Construction 21

3.2.3 Bioreactor Performance Testing 25

3.2.4 Statistical Tests 28

Results 3.3 29

Discussion 3.4 34

CHAPTER FOUR: MANUSCRIPT “A HAND-HELD DEVICE TO APPLY LOADS AT TARGETED MAGNITUDES AND STROKE FREQUENCIES DURING INSTRUMENT ASSISTED SOFT-TISSUE MOBILIZATION” 38

4.1 Introduction 38

4.2 Methods 39

4.2.1 Device Construction 39

4.2.2 Device Performance Tests 40

4.2.3 Experimental Validation 42

4.2.4 Statistical Tests 42
4.3 Results 42
4.3.1 Device Performance Tests 42
4.3.2 Experimental Validation 43
4.4 Discussion 44
CHAPTER FIVE: CONCLUSIONS 47
5.1 Summary 47
5.2 Future Work 47
5.2.1 In -Vivo Device 47
5.2.2 In -Vitro Device 47
REFERENCES 50

LIST OF TABLES

Table 1: Bioreactor design criteria 20

Table 2: Force accuracy test group 1, target force waveform parameters. Each peak force and amplitude combination was tested at each frequency (12 waveforms total) 26

Table 3: Force accuracy test group 2, target force waveform parameters. Each peak force and amplitude combination was tested at each frequency (9 waveforms total) 27

Table 4: Average stroke frequency across all tested loads (0.1-5.0N). The R^2 values are for the Fourier series summation fit of the measured load data. 43

LIST OF FIGURES

Figure 1: Ligaments of the ankle joint [85] 4

Figure 2: Stress–Strain curves representing the mechanical properties of the medial collateral ligaments for sham-operated and healing MLCs at time periods 6, 12 and 52, weeks [86] 6

Figure 3: IASTM tools [87] 8

Figure 4: Deviatoric and dilatational components of a stress tensor 17

Figure 5: Moor's circles and 3D stress elements for (A) tensile stress, (B) compressive stress, (C) and tension + compressive stress 17

Figure 6: Theoretical mechanical loading conditions created by IASTM. The size of the deviatoric stress is increased compared to combined tension/compression due to added shearing forces. 19

Figure 7: Image of bioreactor for force controlled multi-axis stimulation of collagen gels 22

Figure 8: Synchronized tensile and compressive force waveforms 24

Figure 9: Gelatin sample used for validation with 16 mm length (L), 8 mm width (w), and 4.5 mm thickness. Gelatin concentration 1 gram of gelatin per 10 ml of water 25

Figure 10: Sample force waveform with labeled parameters. 26

Figure 11: Sample of a Fourier series curve fit for used for calculating the mean peak and amplitude of the force waveforms during the bioreactor performance tests (R = 0.92) 27

Figure 12: The accuracy of the tensile waveforms averaged over all tested peak forces and grouped by the waveform frequencies (N=40) from test group one using the rubber band sample (*= significant difference). (A) Accuracy of the peak force (* p = 0.000) (B) Accuracy of the amplitude (All groups were significantly different p = 0.000) 29

Figure 13: The accuracy of the tensile waveforms averaged over all tested frequencies and grouped by target peak force (N=40) from test group one using the rubber band sample. (A) Accuracy of the peak force (*p=0.05) (B) Accuracy of the force amplitude (*p = 0.000)..... 30

Figure 14: The accuracy of the tensile and compressive waveforms averaged over all tested peak forces and grouped by the waveform frequencies (N=40) from test group one using the gelatin sample (*= significant difference tension • = significant difference compression). (A) Accuracy of the peak force (* p = 0.05, • p = 0.05) (B) Accuracy of the amplitude (* p = 0.005, • p = 0.001) 31

Figure 15: The accuracy of the tensile and compressive waveforms averaged over all tested frequencies and grouped by target peak force (N=40) from test group one (*= significant difference tension • = significant difference compression). (A) Accuracy of the peak force. (B) Accuracy of the force amplitude (*p = 0.013)..... 32

Figure 16: Accuracy of applied load amplitude for a constant peak load of 0.15N (N=30). (*= significant difference tension • = significant difference compression). (***, *, * p = 0.001, • p = 0.01) 33

Figure 17: Comparison of average accuracy between tensile and compressive waveforms (N=120)..... 33

Figure 18: Accuracy of the force controlled stimulation over six hours of continuous operation. (A) Peak force accuracy (p = 0.000) (B) Force amplitude accuracy (p = 0.000) 34

Figure 19: IASTM device design and components (A) Device components (B) Graston tool (C) Data acquisition and graphical user interface used with the device. 39

Figure 20: Automated calculation of loading parameters. (A) Load data measured by the device during performance testing overlaid with the target loading profile. Black circles represent data included in the calculation of mean stroke force, while open circles were excluded from this calculation. (B) Fourier series fit for measured load data with target frequency of 0.5Hz. Note: the compressive load is applied every half cycle. 40

Figure 21: Experimental setup. A) Device at a 60 deg shaft angle to determine error between the force measured by the device and the compressive load applied to a surface, which is measured by an auxiliary force sensor. B) Device in use during the rodent experiment 41

Figure 22: Results from device performance tests. (A) Comparison between the compressive force measured by the device and the compressive surface force measured by the auxiliary force sensor. A slope of 1 indicates the load measured by the device equals the compressive force applied to the surface. (B) Percent error in mean applied load at each targeted magnitude, averaged for three different operators. * = significantly different from all other targeted forces. 43

Figure 23: Results from experimental validation. (A) Average applied force and (B) average applied stroke frequency across five IASTM treatments for three rats. 44

Figure 24: PTFE molds for collagen gel culture. (A) Empty mold (B) Mold with a cultured fibroblast seeded collagen gel (C) Collagen gel clamped in the bioreactor 48

Figure 25: Proposed force controlled stimulation loading configuration. The loading platen only applies a compression to one half of the sample while the other half only received a tensile load. This allows the comparison of the effect of both loading conditions in one sample 49

NOMENCLATURE

$\boldsymbol{\epsilon}$	Strain
$\boldsymbol{\epsilon'}$	Deviatoric Strain
$\boldsymbol{\epsilon_{dil}}$	Dilatational Strain
$\boldsymbol{\sigma}$	Stress
$\boldsymbol{\sigma'}$	Deviatoric Stress
$\boldsymbol{\sigma_{dil}}$	Dilatational Stress

CHAPTER ONE: INTRODUCTION

1.1 Motivation

Ligaments are bands of dense connective tissue that bind bone to bone to provide joint stability and guide smooth joint articulations. Through excess loading and overuse, ligaments are predisposed to injury. These injuries are accountable for over seven million hospital visits per year, and yearly medical costs of three billion dollars [1,2]. While many ligament injuries heal without intervention, up to 1/3 of patients experience pain and dysfunction for 3 years or more [3]. These lingering symptoms are a consequence of the slow healing process for ligaments, taking as long as one year to regain 50% of their original strength and in some cases never fully recovering to the strength of uninjured tissue [4]. Ligament damage can increase joint laxity and alter joint kinematics, increasing the risk for osteoarthritis, a painful disease that afflicts 27 million people in the United States [3,5].

The functional disabilities associated with injured ligament occur as a result of structural changes in the tissue [6]. Collagen type 1, the main load-bearing protein in ligament, becomes highly disorganized after an injury, in contrast to healthy ligament where the collagen is highly organized. The primary cells that repair and maintain these collagen networks in ligament tissue are fibroblasts. Fibroblast activity is regulated by mechanical stimulation [7] but the specific mechanical environment that is most beneficial to collagen remolding is not completely understood. Still, mechanical stimulation is necessary for complete injury healing as joint immobilization after injury

reduces the strength, stiffness, and size of healing ligament [8,9]. Instrument assisted soft tissue mobilization (IASTM) is a manual therapy technique that can be used to mechanically stimulate ligaments that are palpable through the skin. However, there is limited experimental evidence for the biomechanical and physiological effects of soft tissue mobilization treatments. As a consequence, there is no consensus on the optimal magnitude, duration, and frequency of force that should be applied to injured soft tissue during these treatments.

1.2 Research Goal

The purpose of this research is to develop methodologies to study the specific mechanical loads (e.g. force magnitude, duration, rate, and direction) that strengthen and accelerate ligament healing. This study focused on developing two experimental devices. The first device is for in-vivo testing of IASTM in animal studies. This device was designed to allow the user to target specific force magnitudes and frequencies during IASTM. The second device is a novel multi-axis bioreactor for 3D cellular constructs. This device was designed to apply repeatable force controlled stimulations for a variety of loading conditions.

The technology developed from this study will enable future research projects to identify and describe the specific mechanical environments that promote collagen remodeling and strengthen ligament. This knowledge can give insight into the functional effects and optimal dosage of IASTM, and provide a basis to elucidate extracellular matrix remodeling in all fibroblastic soft tissues. Additionally, the devices developed in this study have the potential to contribute to the field of tissue engineering, where optimal

mechanical stimulation regimes need to be determined for the development of functional tissue surrogates [10,11].

CHAPTER TWO: BACKGROUND

2.1 Ligament

2.1.1 Ligament Structure and Function.

Ligaments are dense bands of connective tissue that stabilize and guide joint articulations (Figure 1). Ligament is a viscoelastic material that exhibits time dependent properties including creep, stress relaxation, and hysteresis [12]. Ligaments structure is a combination of a ground substance, composed of water, lipids, proteoglycans, and other proteins, that is reinforced with a fibrous network of collagen and elastin [4,12]. Scattered among the longitudinally aligned collagen matrix are fibroblast cells [4,13]. Fibroblasts produce, repair, and maintain the extracellular matrix (ECM). Collagen represents approximately 75% of the dry weight of ligament and proteoglycans, elastic, glycoproteins and other proteins make up the remaining 25% [13]. Collagen type one accounts for 85% of the total collagen within ligaments and is the main load bearing

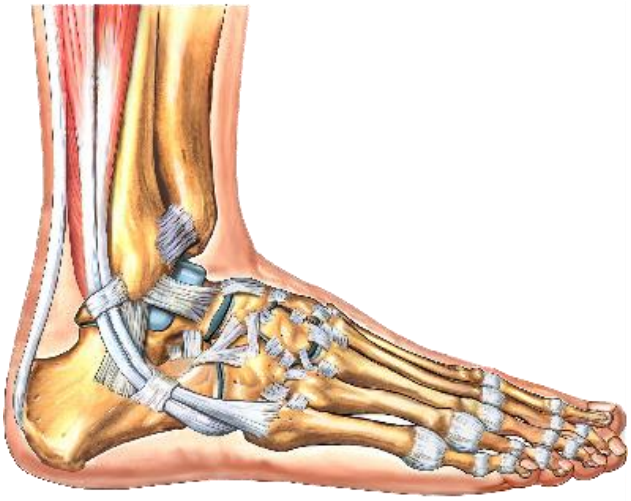

Figure 1: Ligaments of the ankle joint [85]

constituent in the ligament [13]. The collagen fibers are highly aligned which produces non-linear anisotropic mechanical behavior in the tissue.

Ligament tissue primarily supports mechanical loads in tension, but can also experience compression and shear in concentrically loaded ligaments such as the periodontal ligament [14]. Ligaments of the knee are commonly injured [1] therefore the physiological strains of ligaments in the knee have been thoroughly studied. During knee physiologic function, in movements such as side stepping and vertical drop jump, the anterior cruciate ligament (ACL) withstands tensile strains up to 6.1% and forces up to 5% of body weight [15]. After an injury, the ligament can no longer support the same magnitude of mechanical load thus the joint must be supported by its natural articulating geometry, surrounding musculature, and other ligaments. As a result, the strains in surrounding uninjured ligaments can increase after an injury. In the knee joint, with a separated ACL, the strain through the medial collateral ligament (MCL) increases by 1.8% when undergoing tibial translation [16]. Similarly, when the MCL is transected, the strain through the ACL increases by 0.7% during landing from a vertical jump [17]. Lastly, the strains through the injured ligament tissue can increase, because the injured ligament becomes more lax and less stiff after an injury [18].

2.1.2 Ligament Wound Healing

Ligament injuries account for over 7 million United States hospital visits annually [1]. Ligament injuries can be acute, from excess loading, or can occur slowly overtime due to overuse. Ligament healing occurs in three phases: inflammation and blood clot, matrix and cellular proliferation, and remodeling and maturation [12]. The first phase is characterized by the retraction of disrupted ligament ends, formation of a blood clot, and

release of growth factors to signal infiltration of cells. The proliferative phase is defined by hypertrophic fibroblastic cells producing granulation or “scar” tissue in the gap between the ligament ends. The scar tissue is highly disorganized and more vascularized than native ligament tissue. Over the course of a few weeks the collagen is remodeled and becomes better aligned but still does not have the strength or collagen composition of native ligament. Next, the remodeling and maturation phase occurs over months and even years after the initial injury. In this stage, the matrix is continuing to become more like native ligament but still has structural and functional differences including more disorganized collagen networks, altered collagen and proteoglycan composition, 10-20% reduced viscoelastic properties, and 50% reduced strength and stiffness even up to a year after injury [12] (Figure 2).

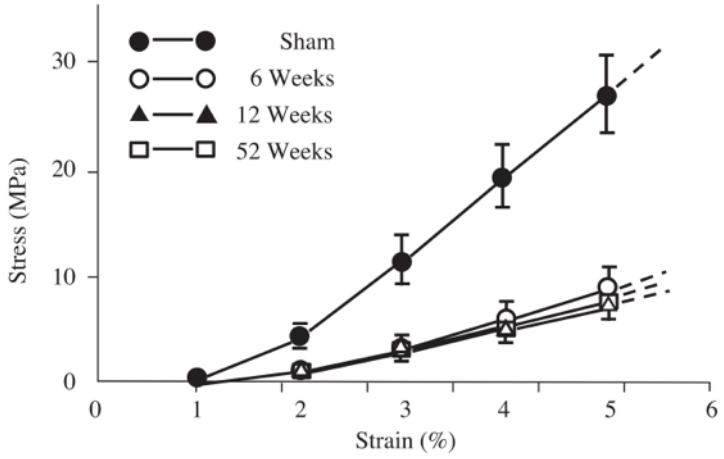

Figure 2: Stress–Strain curves representing the mechanical properties of the medial collateral ligaments for sham-operated and healing MLCs at time periods 6, 12 and 52, weeks [86]

2.1.3 Standard of Care

The current standard of care for most ligament injuries starts with rest, ice, compression, and elevation (RICE) [19]. After the acute inflammatory stage (48-72

hours), the joint is placed in a braced for weeks to months depending on the severity of the strain. Once significant pain has subsided, normal activities can be resumed. However, there is inconclusive evidence for the effectiveness of RICE during the acute healing phase [20]. Other new therapies are in development including ultra-sound, biological scaffolds, and stem-cell treatments [21–23]. While these treatments show promise, they are costly and are more invasive than other more conservative techniques, this limits the broad adoption of these treatments by health care providers. There is evidence that conservative treatments such as supervised physical therapy and manual therapy may be a more effective form of treatment than RICE [24,25]. Manual therapies are less constrained by cost and regulatory oversight and are used by 36 million people in the United States each year [26]. Instrument Assisted Soft Tissue Mobilization is a manual therapy technique that has shown to be effective at reducing pain and accelerating healing in ligament injuries [27,28].

2.2 Instrument Assisted Soft Tissue Mobilization

2.2.1 Origins

Massage therapy has been used for thousands of years as a way to treat musculoskeletal pain. In ancient Greece and Rome, small metallic instruments were used in bathhouses for therapeutic treatments [29]. Similarly, the traditional Chinese therapy known as “gua sha” uses a metal instrument to push or scape the skin and is thought to facilitate the supply of blood and oxygen to stimulated tissue [30]. IASTM is a treatment based on these principals of dynamically stroking damaged tissue with a blunt instrument to facilitate a healing response. IASTM encompasses a variety of techniques with different designations such as augmented soft tissue mobilization (Astym), fascial

Figure 3: IASTM tools [87]

abrasion technique, Graston technique, and sound-assisted soft tissue mobilization [29,31,32]. Historically, tools may have been made from stones or animal bones to apply stimulus, instruments used today are primarily made from stainless steel (Figure 3).

2.2.2 Practical Application

IASTM is a conservative and non-invasive technique [27]. The use of the tool allows the practitioner to maximize the force applied to the tissue with minimal discomfort or fatigue to therapist's hands and upper body compared to other massage therapy techniques [33]. While there is some variation in the technique used between practitioners, the clinical protocol for IASTM will usually contain the following elements: warming of the tissue via exercise or hot pack, 40 – 120 seconds of IASTM therapy on an isolated soft tissue injury, stretching of the injured tissue, strengthening exercises for the joint with the injured tissue, and cryotherapy to reduce any initial onset of pain or excessive inflammation from the treatment. This is repeated 2 times per week for 4 – 6 treatments [34].

2.2.3 Clinical and Biological Effects

In case studies IASTM has been shown to improve function and reduce pain for people with shoulder, Achilles tendon, and patellar tendinopathy [35–37], chronic ankle pain [38], chronic finger pain [28], and lower body muscle strains [39]. In animal studies, IASTM has been shown to accelerate the rate of tissue healing [27], increase the total number, recruitment and activation of fibroblasts in the injured tissue [40,41] and increase the number of tissue-resident mesenchymal stem cells in the arterial ad-ventitia and micro-vessels of the injured tissue by threefold [42]. Because fibroblast originate from mesenchymal stem cells [43], this gives compounding evidence that IASTM is associated with increased fibroblast activity.

2.2.4 Mechanisms

Despite positive clinical outcomes, there are few experimental studies of the mechanisms and functional effects of IASTM on injured tissue. There are two main hypotheses for the functional effect of IASTM. One hypothesis is that the main functional effect of IASTM is the removal of scar tissue adhesions in and around the injured tissue. Scar tissue is thought to limit perfusion to the injured soft tissue, which restricts the supply of oxygen and nutrients, and interferes with collagen synthesis and regeneration of tissue, which can cause incomplete functional recovery of the tissue [2,44]. This hypothesis is supported by animal studies showing increased cellular activity in the tissue [27,40,41] and micro-vasculature in the tissue [29,38,45]. Another hypothesis is that IASTM functions from restarting the healing process by causing localized inflammation in the damaged tissue [29,38]. An adequate amount of inflammation in the tissue can facilitate healing through the signaling of fibroblasts to synthesize collagen [46]. In

addition, soft tissue inflammation has been shown to be associated with increased numbers of fibroblasts. This fact, in combination with studies showing increased fibroblast activity after IASTM [27,40,41], support this hypothesis. However, Vardiman et al. (2014)[47] reported no significant increase in inflammatory signaling after IASTM treatments. A third, less investigated hypothesis, is that the forces produced during IASTM treatments create an environment that signals fibroblasts to remodel the extra cellular matrix and reform strong collagen networks. Fibroblasts have been shown respond to both tensile and compressive mechanical loads [14,48–53]. However, fibroblasts response to more complex loading has not been thoroughly investigated. IASTM treatments create a complex dynamic mechanical environment that involves tensile, compressive, and shearing forces. The in vitro and in vivo devices presented in this study provide frameworks to investigate the effects of complex loading on fibroblast activity and mechanical changes in healing ligament

2.3 Mechanobiology

2.3.1 Mechanotranduction

The fibroblast cells in the ligament are signaled to produce, repair, and maintain the ECM by sensing the mechanical forces transferred through the ECM. This process by which cells convert mechanical stimulus to biochemical activity is known as mechanotransduction [54,55]. The process of mechanotransduction and matrix remodeling is seen is many different musculoskeletal tissues including bone, ligament, muscle, and tendon [54]. Mechanical loading can increase the size and strength of musculoskeletal tissues while the absence of load can cause the tissue structure to become weak [8,9,54,56]. The mechanical environment that the cells experience within

ligament during physiologic function is complex and can include components of force from tension, compression, and shear due to fluid flow throughout the tissue during motion. The macro scale tensile strains in ligament during physiological loading have been well quantified [16,17] but compression and fluid shear mechanical loads have been less investigated. Although the mechanical environment cells experience within native tissue is complex, to clearly understand the effects of mechanical stimuli on mechanosensitive cells and EMC remodeling, the mechanical stimuli applied to the cells must be isolated and precisely controlled.

2.3.2 In –Vitro Experimental Models

The in-vivo environment is extraordinarily complex. As a consequence, the response of cells to mechanical and chemical stimulation has largely been studied using in-vitro cell culture systems. Traditionally, 2D cell cultures have been used as the primary in-vitro experimental model because they provide a simple and efficient method to study cellular responses from mechanical and chemical stimulation [57]. In 2D cell culture, cells are typically mechanically supported in a petri dish or glass polystyrene. While these 2D models have contributed greatly to the understanding of cell behavior, there is growing evidence that the results from these models can deviate significantly from the in-vivo response [57]. In three-dimensional cell culture, cells are suspended in different types of laboratory created ECM. 3D gel models provide a more realistic biochemical and biomechanical microenvironment than a 2D model while still allowing control over culture conditions, specimen composition, and boundary conditions [57–59]. For the modeling of soft tissues, such as ligament and tendon, fibroblasts are often seeded within an ECM made of collagen [53,57,60]. These 3D models are valuable because not

only can the effects stimulation be measured in substrate mechanical properties changes and chemical signaling, changes in the microstructure of the ECM can also be observed [53]. While these models provide an effective experimental tool to understand the effects of mechanical stimuli on cells in a 3D environment, they do not have the same level of structural and composition complexity, nor do they have the mechanical strength of native soft tissues.

A wide variety apparatuses have been developed for the mechanical stimulation of cell and tissue cultures. These devices can apply multiple different mechanical stimuli including: compression (hydrostatic pressure or direct compression), longitudinal stretch, bending, substrate distention, fluid shear stress, and biaxial stretch [61]. Newer devices have sought to apply more complex loading to tissue cultures such as combined tension/compression and compression/shear [62,63]. Other systems have been developed to apply tensile stimulation while also altering the chemical environment around the tissue culture to more closely mimic the in vivo environment [64]. In chapter three of this study a novel multi-axis bioreactor for the stimulation of 3D fibroblast seeded tissue constructs is developed.

2.3.3 In-Vivo IASTM Experimental Models

While the mechanical environment during an in-vivo experimental model cannot be as precisely controlled as the in-vitro environment, in-vivo experiments provide results that are more directly transferable to clinical practice, but still provide quantitative data that cannot be obtained from a clinical study. In-vivo IASTM experiments generally involve three components: chemically or surgically induced soft tissue injury, IASTM treatments applied to injury, and testing (mechanical, biochemical and histological) to

determine functional effect. Despite the fact that variation in pressure applied during IASTM has been shown to affect fibroblast activation [65] and in-vitro studies have shown that both magnitude and rate of force application effect the response of fibroblasts, [49,52,66] few in-vivo studies have even attempted to control the mechanical loads applied during IASTM. This makes it impossible to connect the biochemical and mechanical changes from IASTM to specific loading conditions during the treatment. As a result, there are no quantitative guidelines for the magnitude or rate at which force is applied during the IASTM. This is due in part to the absence of practical tools to control applied forces during IASTM and other massage treatments.

Multiple techniques and devices have been utilized to control applied force during soft tissue mobilization. One technique was to use an IASTM tool on a force plate prior to treating the subject to get a kinesthetic feel for the amount of pressure applied [27,67]. This technique allows for some qualitative control but provides no feedback during the treatment and does not measure the applied force. Devices using pressure transducers have been developed to evaluate pressure applied during treatment, but these devices offer no feedback to control pressure or frequency [40,68]. Zoest et. al. [69] presented a handheld device that measured contact forces during massage using a 3D piezoelectric strain gauge. However, the device had problems with force drift and measurement accuracy and did not give the practitioner any feedback during treatment to control the force applied. Tuttle et. al. presented a device that did provide feedback during massage but was limited to use in massage using the finger tips. However, these handheld devices [69,70] were not designed for IASTM treatments, instead they were intended for use during muscle tissue massage.

Other researchers have made robotic systems to measure force during massage. Wang et. al developed a robotic system that applies massage like strokes using a stainless tip and controls for compressive force using a feedback loop [71]. The device moves along two axes, in the x and z directions but only controls for the compressive force. Additionally, animals are required to be strapped down in a specific position next to the device base in order to have the force properly applied. Similarly, Zeng et al[72] developed a pneumatic system to control the applied force during compressive and lengthwise strokes. The device used a metal roller, or "kneading wheel", to apply the force across the muscle tissue and was design for use with rabbits. Both of these devices could accurately control force but they do not replicate the IASTM protocols utilized in clinical settings because they only focus on muscle tissue massage as opposed to soft tissue treatments [71,72]. In addition, they require specific positioning of animal subjects and as such are limited in their ability treat different joints. In chapter three of this study, a practical hand-held device is presented that allows for the user to accurately control both force and frequency during IASTM treatments. This tool provides the basis for future in-vivo experiments on the optimal mechanical loads that should be applied during IASTM.

CHAPTER THREE: MULTI-AXIS MECHANICAL STIMULATION BIOREACTOR FOR STIMULATION OF 3D CELLULAR CONSTRUCTS

3.1 Introduction

3.1.1 Mechanical Stimulation of Fibroblasts

There are numerous factors that can be manipulated when applying mechanical stimuli to cells including: axis of loading, dynamic or static loading, load magnitude, frequency, and total duration. Tension has been the primary axis of stimulation studied for the fibroblast based 3D in-vitro models [49,51,53,58,59,73–75]. These in-vitro models have shown that fibroblasts will remodel collagen fibers within the ECM to align along the axis of tensile stress [53,58,59]. In addition, dynamic mechanical stimulation increased construct stiffness, collagen production, and cell viability more than static stimulation [49,51,52,74,75]. Furthermore, peak applied strains between 2.5 – 5% and frequencies between 0.1 – 0.5 Hz were found to be optimal for increased construct stiffness [49,52]. Lastly, continuous dynamic strain without any period of rest, was found to be detrimental to construct stiffness and cell viability [49,52]. Compression has received less attention despite its critical role in the mechanobiology of fibroblasts in fibrocartilaginous and concentrically loaded ligament tissue. Dynamically applied hydrostatic pressure and confined compression of fibroblasts have shown increased gene expression for some collagen proteins and increased cell viability [14,48]. The effects of more complex loading on fibroblasts is still unknown.

3.1.2 Quantifying Mechanical Stimuli

The current approach for evaluating how fibroblasts respond to mechanical stimuli is to apply a specific magnitude of strain in one axis. However, this approach does not completely quantify the stress states that are applied to the tissue construct or the cells. In this study, we aim to describe the stimulation applied to cells in terms of deviatoric stress (shear stress) and dilatational stress (volumetric stress). The rationale for this approach comes from evidence that shear stress is the primary driver of physical phenomena such as material yielding. Through experimentation on ductile materials, deviatoric strain energy or distortion energy has been shown to be the primary factor for predicting material yielding [76]. However, in fibroblasts the effects of deviatoric vs dilatational stress on collagen synthesis and ECM remodeling have not been decoupled.

3.1.3 Deviatoric vs. Dilatational

Any strain or stress tensor can be described in terms deviatoric and dilatational components. When the deviatoric and dilatation components are added together they give the original tensor back (Eq. 1-4). Deviatoric strain is the component of strain that describes a shape change at a constant volume, while dilatational strain is the component of strain that describes a volume change. Similarly, deviatoric stress is the component of stress that causes shape change at a constant volume and dilatation stress is the component of stress that causes volume change (Figure 4).

$$\boldsymbol{\epsilon = \epsilon' + \epsilon_{dil}} \quad \textbf{(1)}$$

$$\boldsymbol{\epsilon_{dil} = \frac{\epsilon_{11}+\epsilon_{22}+\epsilon_{33}}{3}} \quad \textbf{(2)}$$

$$\boldsymbol{\sigma = \sigma' + \sigma_{dil}} \quad \textbf{(3)}$$

$$\sigma_{dil} = \frac{\sigma_{11}+\sigma_{22}+\sigma_{33}}{3} \quad (4)$$

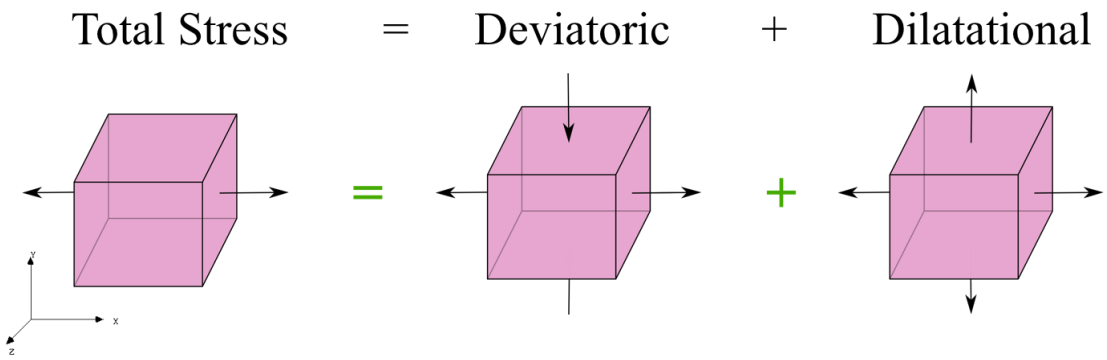

Figure 4: Deviatoric and dilatational components of a stress tensor

Even though deviatoric stress is related to deviatoric strain, in anisotropic materials the strain produced by a pure deviatoric stress is not a pure deivatoric strain. In anisotropic materials predicting the strain would require an accurate measure of the Poisson's ratio of the material so that specific levels of deviatoric and dilatational strain could be predicted and targeted in an experiment. Because most 3D in-vitro constructs for ligament have a fibrous structure composed of collagen similar to ligament they have

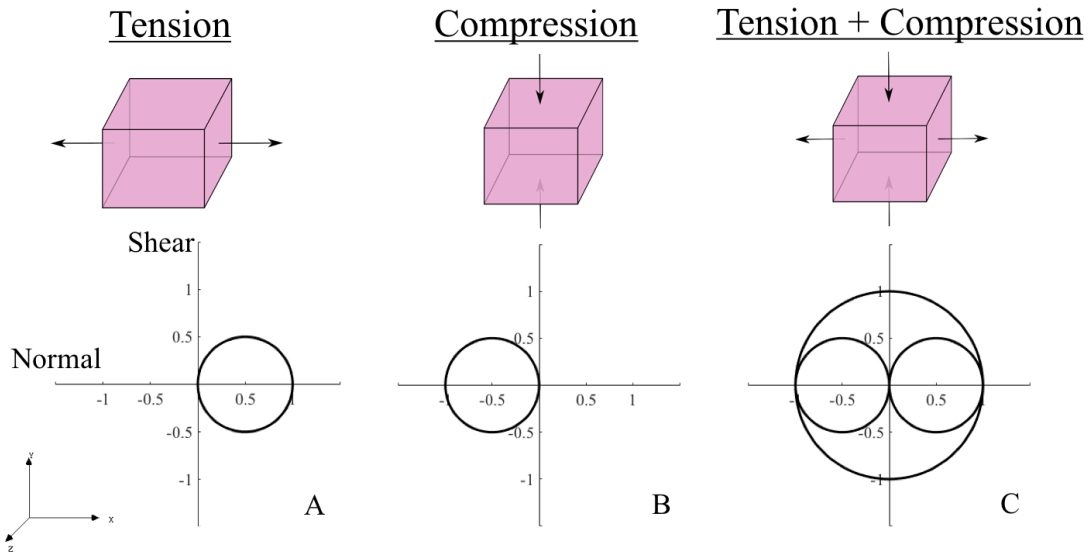

Figure 5: Moor's circles and 3D stress elements for (A) tensile stress, (B) compressive stress, (C) and tension + compressive stress

anisotropic material behavior. Additionally, matrix strain transmission to cells has been shown to vary based on the structure and material properties of the of the ECM in 3D in-vitro constructs made from collagen and fibrin gels [77–79]. Consequently, accurately controlling the deformations of the tissue construct and the cells inside would be challenging and require a multiscale approach to verify the accuracy of the applied strains and the strain transmission from the tissue construct to the implanted cells. However, the traction forces on the cells from the ECM in collagen gels has been shown to be independent of the ECM density and stiffness [77]. This is significant because the stress applied to the tissue construct will be the same stress applied to the cells within the construct. Therefore, using a stress control approach will allow the stress states applied to the ECM to be accurately quantified. Additionally, specific deformations during IASTM cannot be targeted but applied stress can be controlled. Thus, the results from a stress controlled in-vitro model would be more transferable to a controlled in-vivo experiment

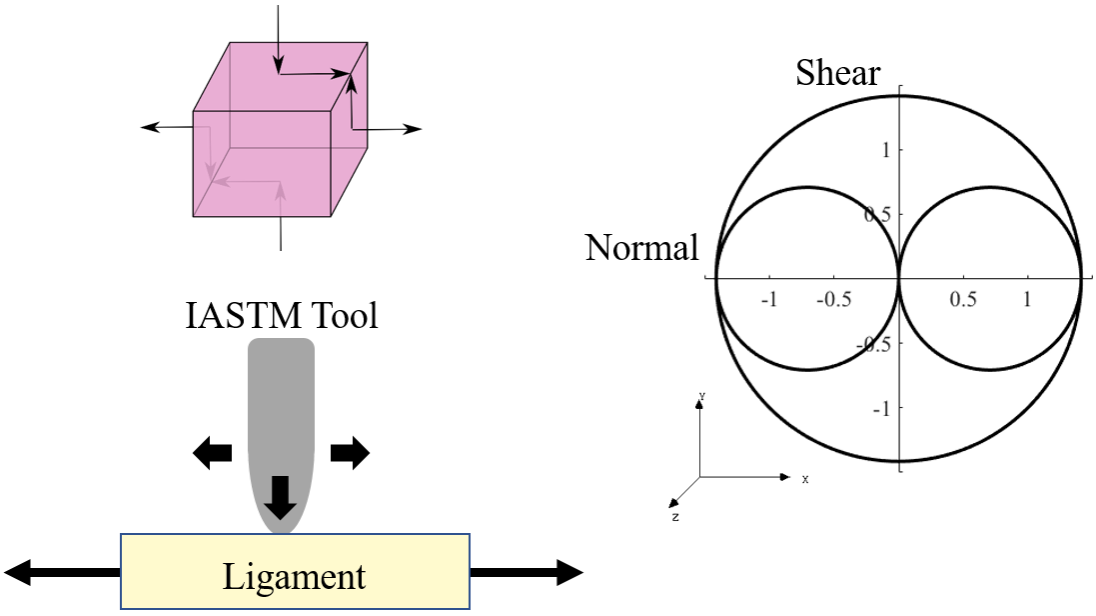

Figure 6: Theoretical mechanical loading conditions created by IASTM. The size of the deviatoric stress is increased compared to combined tension/compression due to added shearing forces.

. From principals of mechanics, it can be shown that a one-dimensional tensile stress and one-dimensional compressive stress will produce the same magnitude of out of plane deviatoric stress (Figure 5 A, B). Applying a tensile and compressive stress of the same magnitude increases the out of plane deviatoric stress by two-fold and creates a purely deviatoric stress, while the magnitude of the normal tensile stress remains the same (Figure 5 C). Accordingly, the effects of deviatoric stress could theoretically be compared through looking at the effects of both loading configurations, pure tensile stress, and combined tensile/compressive stress. While the in-situ forces produced by IASTM have not been accurately quantified, from visual observation, the association can be made that IASTM produces a highly deviatoric stress state due to the applied compression and shear from the IASTM tool and the natural tension from the ligament tissue (Figure 6).

The objective of this study was to design and validate a multi-axis mechanical stimulation bioreactor that can accurately apply tensile and combined tensile/compressive stress states to 3D fibroblast seeded tissue constructs.

3.2 Methods

3.2.1 Bioreactor Design Criteria

There were numerous design criteria specified for the bioreactor (Table 1)

Table 1: Bioreactor design criteria

Design Criteria	Rationale
Accurately controls simultaneous application of cyclic tensile and compressive load to 3D Gels at loads magnitudes between 0 – 1N and frequencies between 0 – 1Hz	The highest failure force (N) seen in the literature for collagen gel constructs was approximately 0.85N [49]
Can operate for 6 hours per day for up to 14 days	~14 days is the average duration of stimulation for cell seeded tissue constructs in the literature [49,50,52]
Can perform uniaxial on tensile test samples using displacement control	Necessary to mechanically characterize tissue constructs and determine functional effects of stimulation
Can fit inside of a standard incubator and withstand environmental conditions (40 x 40 x 50 cm, 37℃, 99% Humidity, and 5% CO_2)	In order to maintain cell viability during stimulation samples need to be an incubator environment
Tissue stimulation chamber must be able to withstand sterilization techniques and maintain sterility during use.	In order to prevent contamination during cell culture the chamber must be properly sterilized
Tissue stimulation chamber must allow the sample to be covered in cell culture media during stimulation	In order to maintain cell viability and prevent contamination the tissue

	constructs must be covered in cell culture media during stimulation
Tissue stimulation chamber can accommodate varying sample sizes	Allows flexibility for the device to be used for stimulating and mechanically testing samples of different size and material

3.2.2 Bioreactor Construction

The bioreactor is primarily composed of plastic or corrosion resistant metal to prevent corrosion and withstand ethylene oxide sterilization (Figure 7). The base plate, sample chamber supports, and shaft connecting horizontal load sensor to the grip were machined from polyoxymethylene (acetal) plastic. The clear plastic components connecting the load sensors to the actuators and the outer walls of the sample chamber were machined from acrylic. All black plastic components were 3D-printed using Polylactic acid (PLA) filament. The support structure for the compressive actuator and the shaft between the vertical load sensor and loading platen was machined from 304 stainless steel. The loading platen and the white plastic covering the compressive loading platform are made from PTFE. All screws used in the tissue stimulation chamber are nylon, while all other screws are 304 stainless steel.

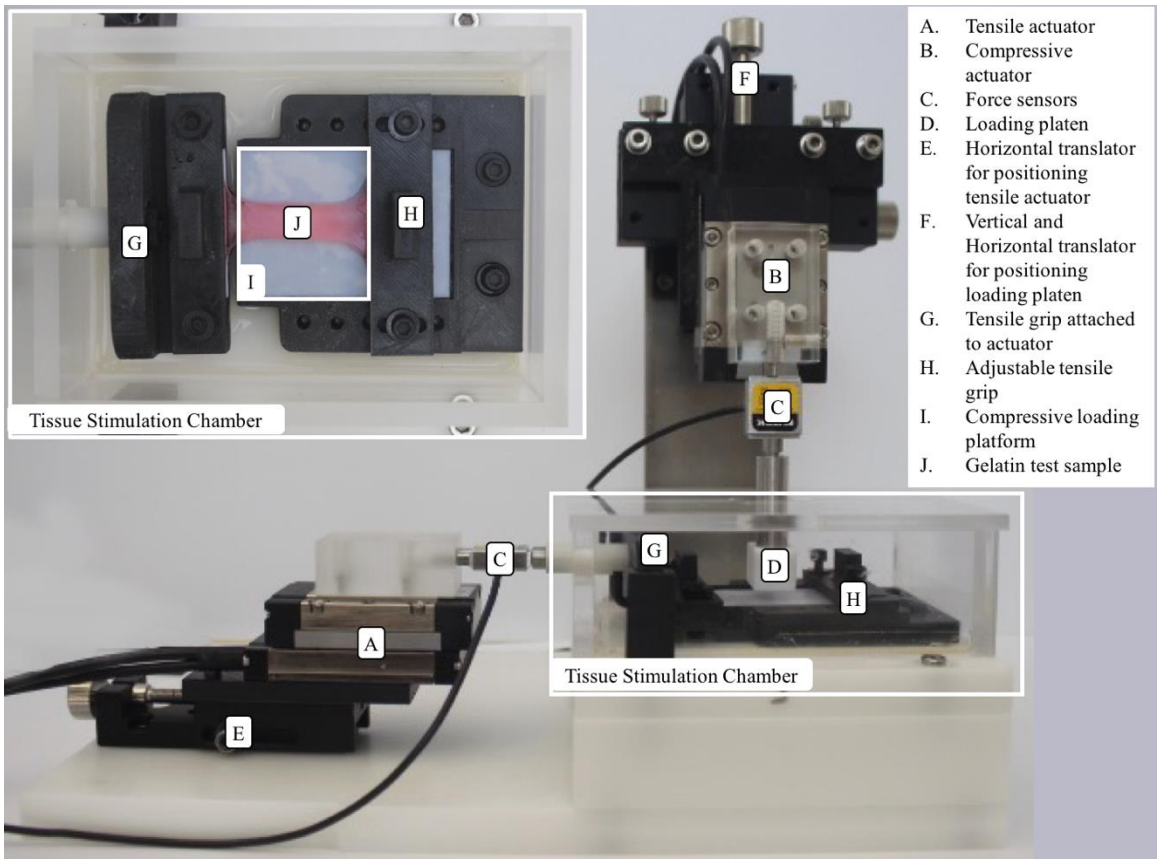

Figure 7: Image of bioreactor for force controlled multi-axis stimulation of collagen gels

The tensile and compressive assemblies are driven by high precision voice coil actuators (SLA-25-010-55-1, SMAC, Carlsbad, CA). Voice coil actuators were chosen because, unlike standard gear driven actuators, voice coil actuators have no mechanical components driving the motion of the actuator. Thus, they have no backlash and are ideal for applications involving long duration cyclic motion because the internal components experience minimal wear overtime. This particular voice coil actuator was selected for its range of motion (10mm), range of force (4N peak, 1N continuous), and high-resolution positioning (1µm). The actuators are powered via a 24V power supply (Keysight E3631A) and 2 single axis amplifiers (LAA-5, SMAC, Carlsbad, CA). Connected to the

tensile and compressive actuators are LRM200 force sensors (1N capacity, FUTEK Inc., Thomas, Irvine, CA) used to monitor the applied force to the specimens.

The tensile actuator is rigidly held to a manually adjustable horizontal translator via a 3D printed connector plate for flexibility in positioning the grip attached to the specimen. The tensile shaft is connected to through the wall of the tissue stimulation chamber and secured to the tensile grip via nylon set screw. The adjustable tensile grip has four fixed-position threaded holes to that allows specimens between 10 – 40 mm in length to be accommodated using the same grip. The tensile grips interface with the specimens by directly compressing the ends of the sample between a stationary base and top clamp secured via nylon screws. The compressive actuator is rigidly held to the manually adjustable two-axis translator to allow flexibility in positioning the compressive loading platen. The loading platen is secured to the load cell via a threaded shaft and a set-screw. The sample rests upon the compression platform. The compression platform surface is covered with a PTFE sheet, secured using cyanoacrylate, to provide a bio-inert surface for the specimens to be stimulated and to reduce friction during compressive and tensile loading. The loading platen interfaces with the sample via manual adjustment of the platen onto the surface of the sample using the translator attached to the compressive actuator.

The bioreactor controls were programmed using LabVIEW Professional Development Software and the Soft Motion Module. The actuators were controlled using a Compact-Rio 9024 and two NI9514 servo interface drives (National Instruments Co., Austin, TX). Force measurements were recorded using a four channel NI9269 strain

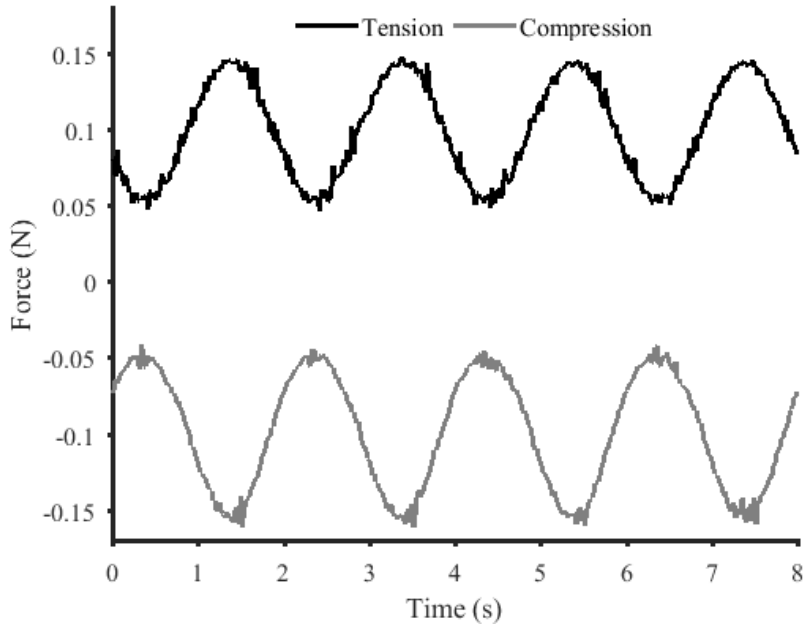

Figure 8: Synchronized tensile and compressive force waveforms

gauge module. Force controlled stimulation was achieved through a custom program. The stimulation is initiated by sending two synchronized sinusoidal position waveforms at user specified displacement for each waveform, one to the tensile actuator and one to the compressive actuator. In order to create a purely deviatoric stress state from a synchronized tensile and compressive stress, the waveforms were sent so that the peak compressive force and the peak tensile force are reached at the same time (Figure 8). The program monitors the max peak force and the minimum peak force reading for each force waveform one time every cycle and shifts the start position and amplitude of each of the position waveforms simultaneously until the peak force reading is within a user specified threshold of the target force value. The force waveforms are fit with a smoothed cubic spline prior to calculating the peak force values to reduce the effects of load cell noise and vibration on the sensitivity of the position waveform shifting. The waveform shifting logic can be turned on or off at any time and the program can simply be used to monitor

the position and force waveforms. This allows the system to seamlessly switch between position or force controlled stimulation. In addition to cyclic stimulation, the system can also be used in displacement control for uniaxial mechanical testing of specimens.

3.2.3 Bioreactor Performance Testing

Three experiments were conducted to assess the performance of the bioreactor. Gelatin samples in a dog bone shape were created to conduct all validation tests (Figure 9). Gelatin was chosen because it can easily be created with varying geometry and numerous samples can be made quickly.

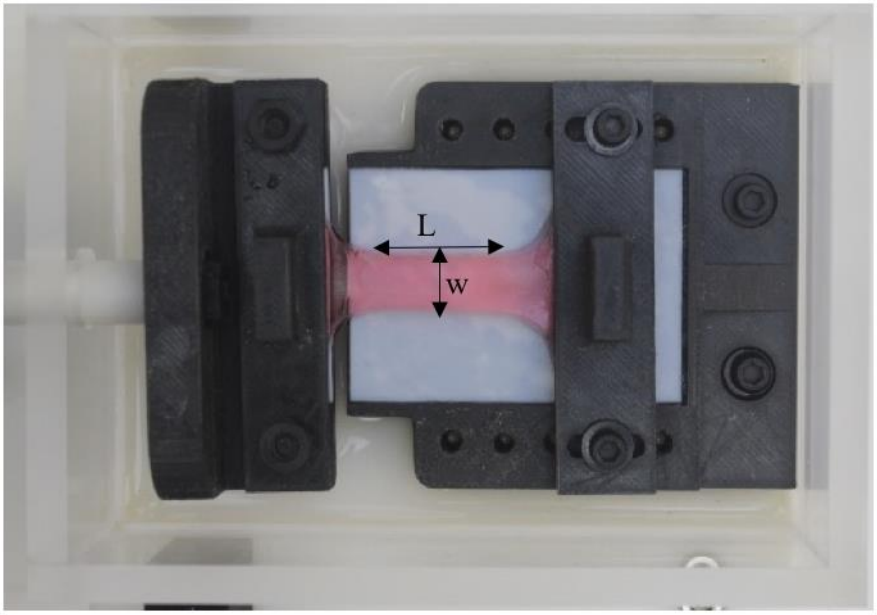

Figure 9: Gelatin sample used for validation with 16 mm length (L), 8 mm width (w), and 4.5 mm thickness. Gelatin concentration 1 gram of gelatin per 10 ml of water

The first test evaluated the accuracy of the force controlled stimulation. Two test groups of tensile and compressive force waveforms were evaluated where the frequency, peak force, and amplitude of the waveforms were manipulated (Figure 10).

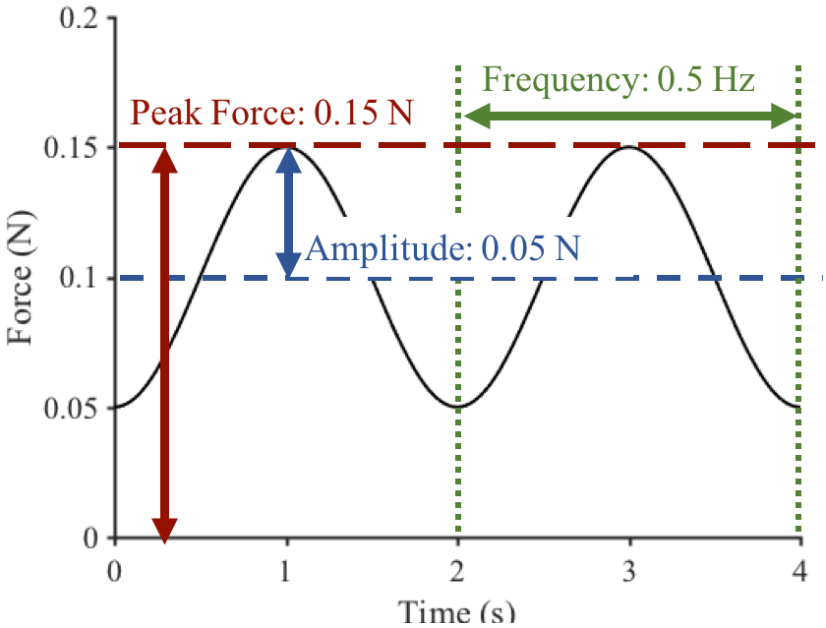

Figure 10: Sample force waveform with labeled parameters.

The first group tested waveforms with peak forces ranging from 0.05 – 0.2 N and frequencies from 0.25 to 1 Hz (Table 2).

Table 2: Force accuracy test group 1, target force waveform parameters. Each peak force and amplitude combination was tested at each frequency (12 waveforms total)

Peak Force | Amplitude (N)	Frequency (Hz)
0.05 | 0.025	0.25
0.1 | 0.05	0.5
0.15 | 0.075	1.0
0.2 | 0.1	

The first test group was performed using a rubber band sample in addition to the gelatin sample, but only the tensile waveform was applied to the rubber band sample to measure the performance of the system using a non-viscoelastic material. The second group targeted a constant peak force while changing the amplitude to isolate the effects of changing force amplitude on accuracy (Table 3).

Table 3: Force accuracy test group 2, target force waveform parameters. Each peak force and amplitude combination was tested at each frequency (9 waveforms total)

Peak Force| Amplitude (N)	Frequency (Hz)
0.15 | 0.025	0.25
0.15 | 0.05	0.5
0.15 | 0.075	1.0

For each test, the force controlled stimulation program was first allowed to reach equilibrium. Equilibrium was defined as the point at which both force waveforms were within 0.01N of their target for at least five cycles. Force measurements were recorded for 30 cycles at each target force waveform, for a total of nine trials. A Fourier series summation was used to fit the force measurement data with a non-linear least squares fitting method [80] every three cycles, yielding ten fitted curves for each trial. The peak

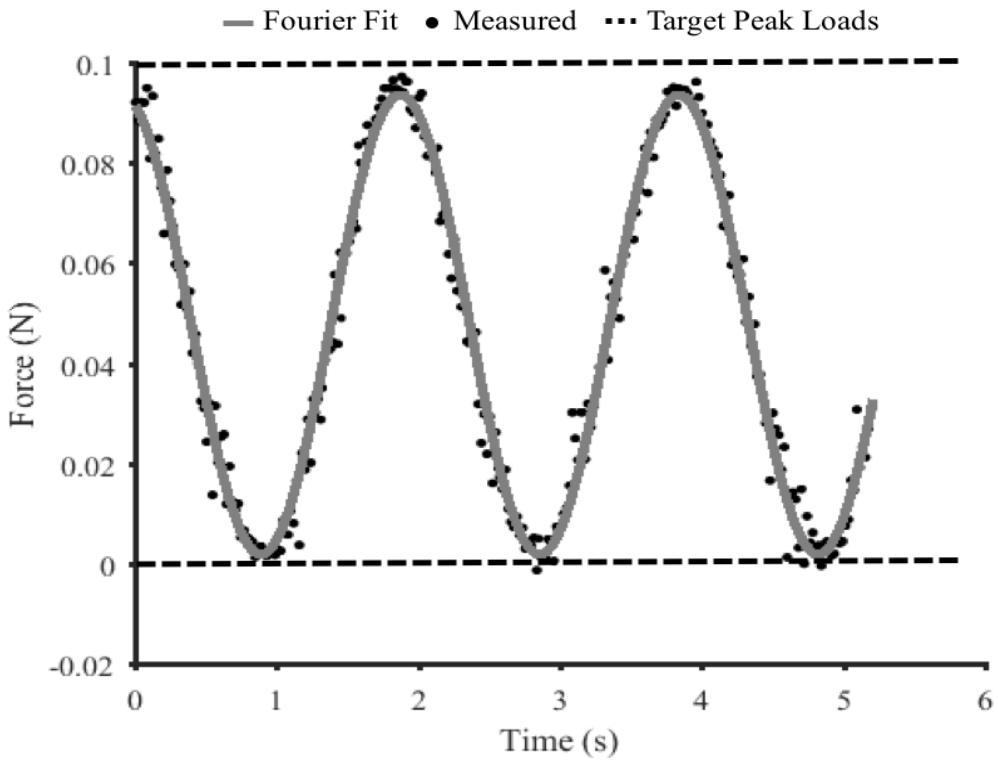

Figure 11: Sample of a Fourier series curve fit for used for calculating the mean peak and amplitude of the force waveforms during the bioreactor performance tests (R = 0.92)

force and amplitude for each trial were determined directly from the fitted curve and the mean for each trial was determined by taking the mean peak and amplitude of each of the ten fitted curves (Figure 11). The error of the peak and amplitude of each trial was defined as the absolute value of the difference between the target force and the measured force ($|Force_{measured}-Force_{target}|$).

The second test evaluated the repeatability of the force controlled stimulation over a long duration. The bioreactor ran for six hours (10800 Cycles) with target force parameters of 0.5Hz, 0.15N peak force, and 0.07N amplitude. Force measurements were recorded for 1800 cycles every hour of operation.

The third test observed the average number of cycles it takes for the force controlled stimulation to reach equilibrium. The force waveform parameters were a frequency of 0.5Hz, peak force of 1N, and amplitude of 0.045N. Ten trials were performed and the number of cycles at equilibrium was recorded for each trial.

3.2.4 Statistical Tests

The effect of frequency and target peak force on the peak force and force amplitude error were analyzed using one-way ANOVA tests with Games-Howell post hoc tests to account for unequal variance between test groups. The effect of target force amplitude on force amplitude error was also examined using one-way ANOVA tests and Games-Howell post hoc tests. The overall error in applied peak force and force amplitude for tensile and compressive force waveforms was compared using a one-way ANOVA. The effect of time point on load error was analyzed using a repeated measures ANOVA with a Bonferroni post hoc test. For all statistical tests, significance was set at $p<0.05$

Results 3.3

From test group one, using the rubber band sample in only tension, the average error of the peak forces and force amplitudes across all waveform frequencies was less than 0.003N (Figure 12). The average error of the peak forces and force amplitudes across all waveform peak forces was less than 0.003N (Figure 13).

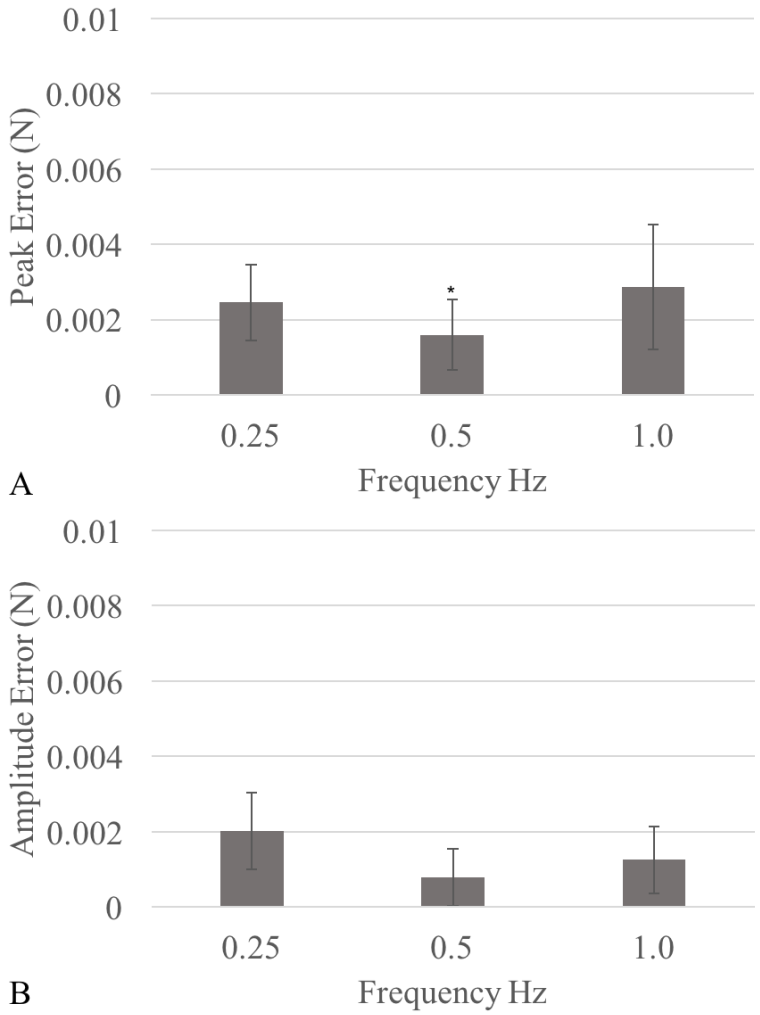

Figure 12: The accuracy of the tensile waveforms averaged over all tested peak forces and grouped by the waveform frequencies (N=40) from test group one using the rubber band sample (*= significant difference). (A) Accuracy of the peak force (* p = 0.000) (B) Accuracy of the amplitude (All groups were significantly different p = 0.000)

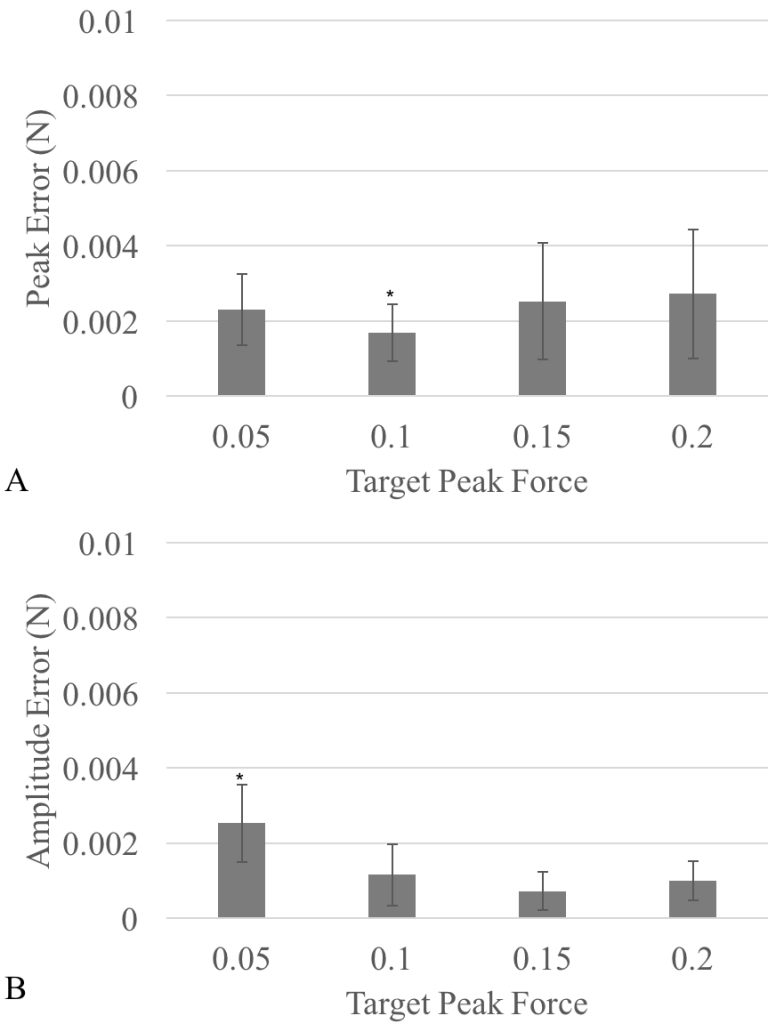

Figure 13: The accuracy of the tensile waveforms averaged over all tested frequencies and grouped by target peak force (N=40) from test group one using the rubber band sample. (A) Accuracy of the peak force (*p=0.05) (B) Accuracy of the force amplitude (*p = 0.000)

From test group one, using the gelatin sample, the average error of the peak forces and force amplitudes across all waveform frequencies was less than 0.005N (Figure 14). For both peak force error and force amplitude error was significantly lower at 0.5Hz for tension and compression (Figure 14). The error of applied peak force was less than 0.005N for all target peak forces (Figure 15). There were no significant differences

between the peak error of all the tested peak forces (Figure 15A). The error of the amplitude was less than 0.005N across all tested peak forces (Figure 15B).

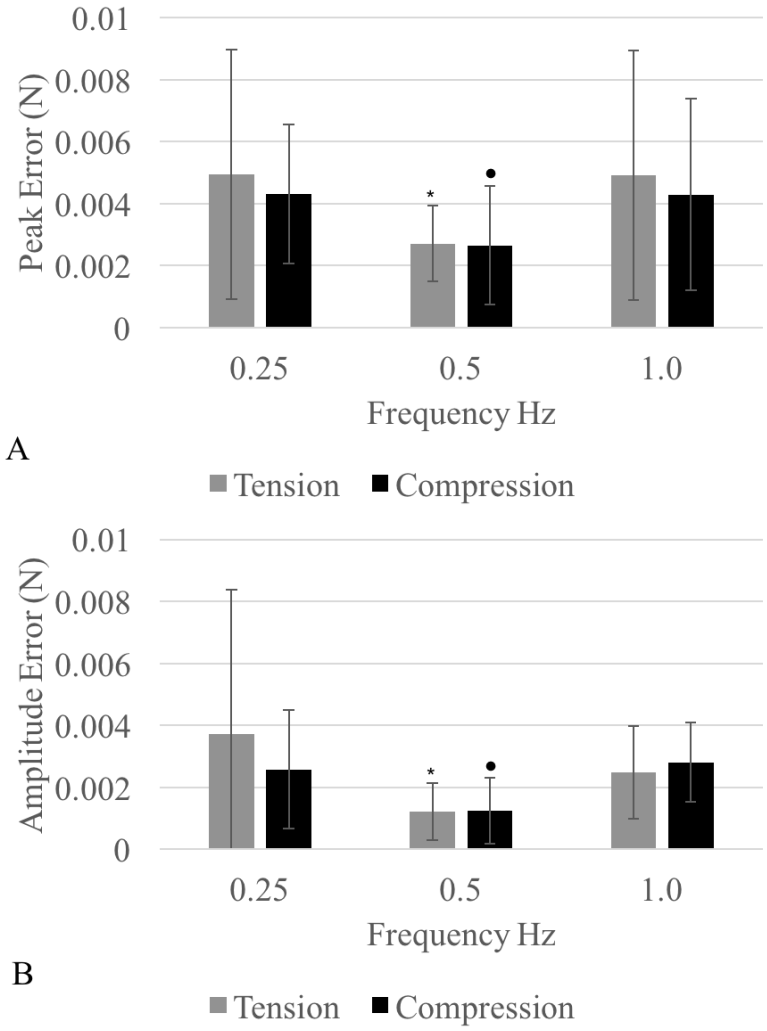

Figure 14: The accuracy of the tensile and compressive waveforms averaged over all tested peak forces and grouped by the waveform frequencies (N=40) from test group one using the gelatin sample (*= significant difference tension • = significant difference compression). (A) Accuracy of the peak force (* p = 0.05, • p = 0.05) (B) Accuracy of the amplitude (* p = 0.005, • p = 0.001)

The error of amplitude for an applied tensile peak force of 0.05N was significantly higher than the other peak forces (Figure 15B) p = 0.013). There were no

significant differences between the tensile or compressive average peak force or amplitude error (Figure 16).

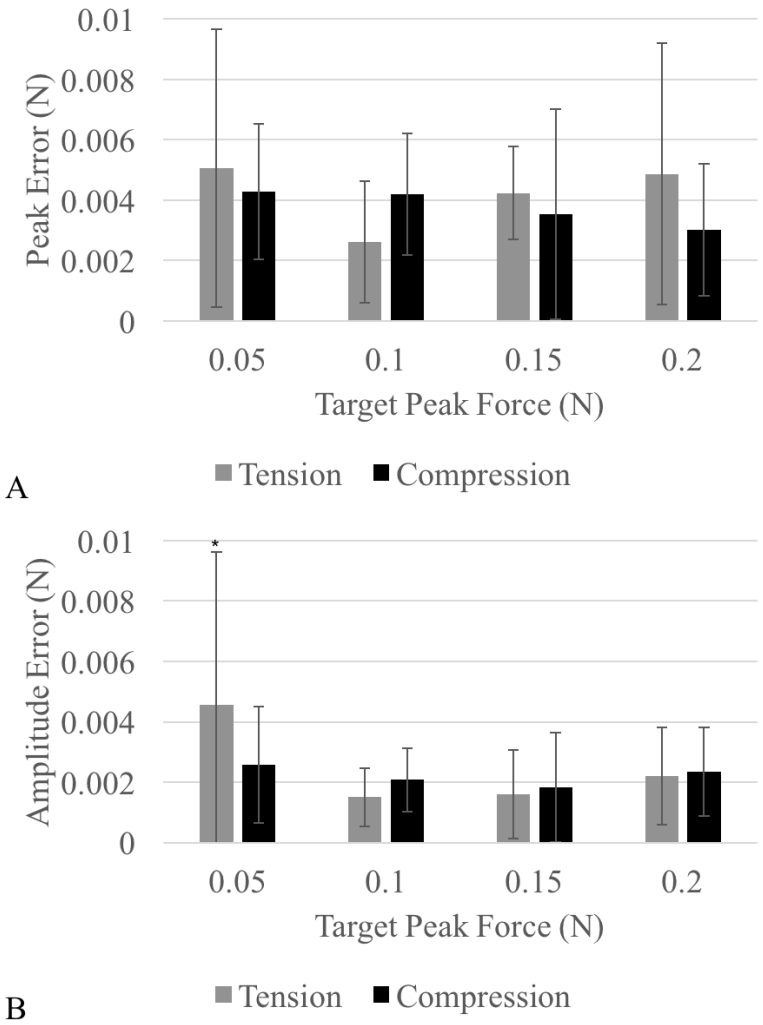

Figure 15: The accuracy of the tensile and compressive waveforms averaged over all tested frequencies and grouped by target peak force (N=40) from test group one (*= significant difference tension • = significant difference compression). (A) Accuracy of the peak force. (B) Accuracy of the force amplitude (*p = 0.013)

The error of the force amplitude while the peak load was held constant was also below 0.005N for all tested load amplitudes (Figure 17). Both the tensile and compressive waveforms were most accurate for a target amplitude of 0.075N (Figure 17).

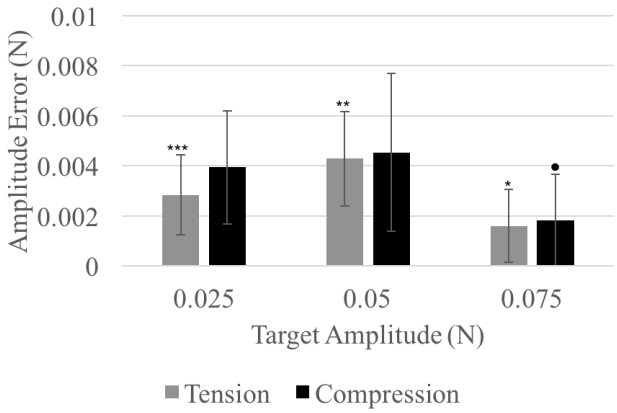

Figure 16: Accuracy of applied load amplitude for a constant peak load of 0.15N (N=30). (*= significant difference tension • = significant difference compression). (*, *, * p = 0.001, • p = 0.01)**

The force control stimulation remained accurate to within less than 0.01N for peak force and amplitude over all time points (Figure 18). The compressive peak error was significantly better on the fifth hour of the test (Figure 18, p = 0.000). The tensile

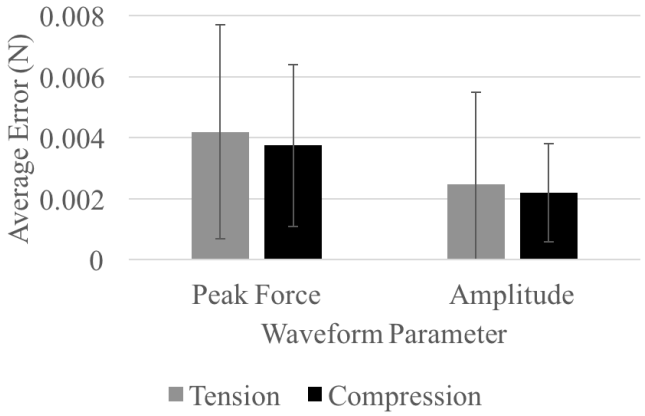

Figure 17: Comparison of average accuracy between tensile and compressive waveforms (N=120)

amplitude error was significantly better at the beginning of the test (Figure 18, p = 0.000).

The mean number of cycles it took for the force controlled stimulation to reach equilibrium was 65.3 ± 9.2 cycles.

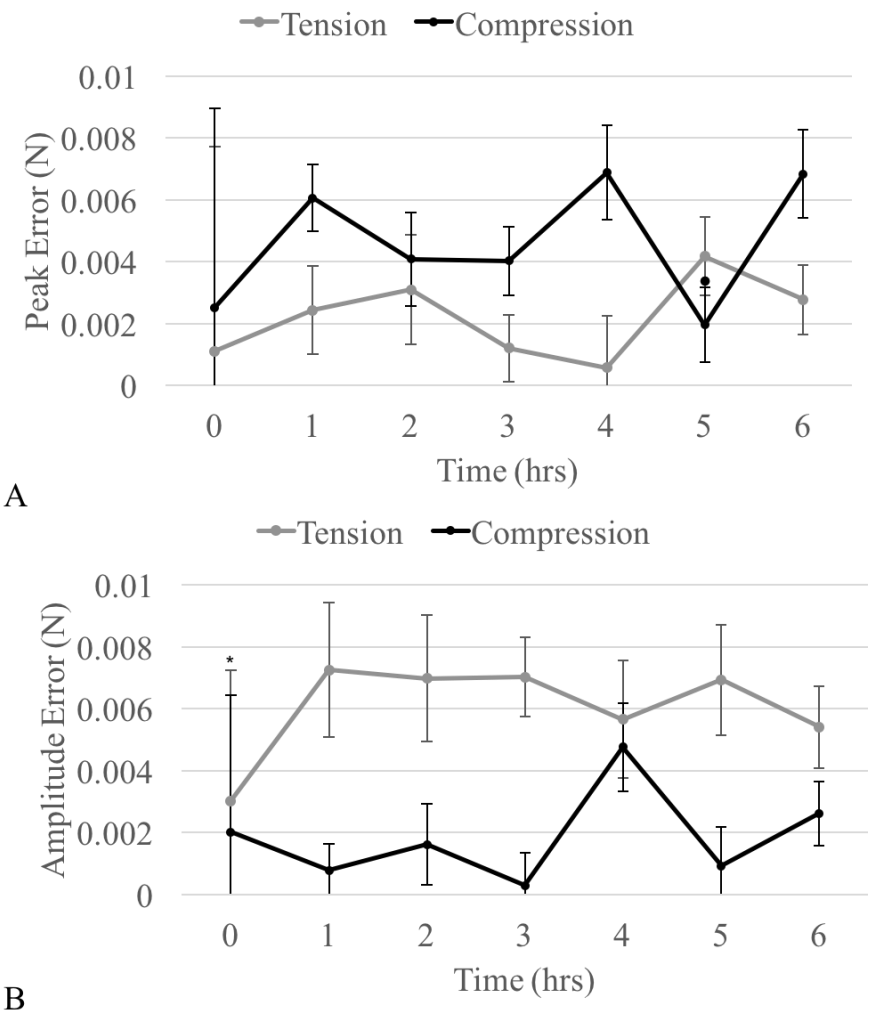

Figure 18: Accuracy of the force controlled stimulation over six hours of continuous operation. (A) Peak force accuracy (p = 0.000) (B) Force amplitude accuracy (p = 0.000)

Discussion 3.4

The purpose of this study was to develop and validate a multi-axis bioreactor to apply force controlled stimulation to fibroblast seeded tissue constructs. The bioreactor was successful in satisfying almost all of the design criteria. It was able to control the application of cyclic synchronized tensile and compressive loads between 0 – 0.2N at frequencies between 0.25 – 1Hz with an error of approximately 0.005N for gelatin samples. The bioreactor was able to reach equilibrium in less than 100 cycles and

maintain consistent force application for a six-hour period. The device fit inside of an incubator and was constructed from materials that can be sterilized with ethyl alcohol. The tissue stimulation chamber was able to fit samples between 10 – 40mm.

The average error of applied force in tension using the rubber band was lower than the error using a gelatin sample, 0.003N vs. 0.005N (Figure 13, 15). Additionally, the largest standard deviation in force error for the rubber band test group was approximately 0.002N lower than for the gelatin sample test group (Figure 13 & 15). The rubber band has linear elastic material properties that create a consistent force response and overall less disturbance in the force control system. The increase in error when testing the gelatin was expected because the visco-elastic properties produce a time dependent force response for which the force control system must compensate. This test demonstrates one of the challenges of designing a control system that is not only stable but also accurately controls the forces applied to visco-elastic materials such as soft tissues. The force control system does not directly control the current signal to the actuators based off of force feedback, rather it adjusts the position set point sent to a position control loop based on the peak load and amplitude of the force waveform measured from applying the specific position waveform. As a result, only the peak and amplitude of the force waveform are controlled. A direct approach to force control could be used to control the complete force waveform applied to the sample; however, this would require a more sensitive load sensor and a higher speed execution rate to compensate for the visco-elastic response of the material. Additionally, the explicit approach would be much more susceptible to instability due to factors such as vibration and variable material properties. Given that the system is used for force controlled

stimulation applied for up to 6 hours at a time, system stability is critical. Thus a more stable system that only controls the peak and amplitude of force application was used as the primary force control method.

To our knowledge, this is the first bioreactor that can apply synchronized multi-axis stimulation in force control. Other multi-axis bioreactors have been developed to apply synchronized multi-axis stimulation [62,63]. While these devices measure the force applied to the tissue constructs, they cannot control the force they apply to the tissue; therefore, they cannot control the stress state applied to the tissue. A drawback of the device is that it can only stimulate one sample at a time. Given that the most in-vitro stimulation experiments take between 7 – 28 days to complete [49,52,53] this will hinder the experiment sample size that could be tested using the device in a feasible period of time. However, the device is small enough that it could be replicated to have multiple chambers operating in a single incubator.

This study has limitations. The error of the force control above 0.2N was not evaluated because the gelatin samples tested were not strong enough to withstand cyclic application of loads greater than 0.2N. However, the force production capacity of the servo actuators is 4N of peak force; therefore, there was greater concern that the system would perform poorly at lower magnitudes of applied force. Further validation could be performed with a stiffer gel material to verify that the device could be used to forces greater than 0.2N. Additionally, while the displacement sequences for mechanical tests have been programmed and verified for functionality, the device was not used for any uniaxial tensile tests on fibroblast seeded tissue constructs. These tests will be performed in future experiments using the bioreactor. Furthermore, there is concern that the friction

from the loading platen and the compression platform could significantly alter the stress state applied to the sample. While the frictional effects have been mitigated through submerging the compression platform in fluid during testing, fixating a PTFE sheet to the compression platform, and machining the loading platen from PTFE the frictional effects have not been quantified and would require further validation.

In conclusion, this study developed a multi-axis bioreactor that can apply force controlled stimulation to samples with a high degree of accuracy and precision. While the device performance has been validated outside of the incubator environment, the device still needs to be tested during an actual in-vitro experiment. Future work will focus on using the device to stimulate tissue surrogates to validate the device performance and to investigate the effects of deviatoric stress on structural and functional changes in 3D in-vitro gels.

CHAPTER FOUR: MANUSCRIPT "A HAND-HELD DEVICE TO APPLY LOADS AT TARGETED MAGNITUDES AND STROKE FREQUENCIES DURING INSTRUMENT ASSISTED SOFT-TISSUE MOBILIZATION"

4.1 Introduction

Ligament and tendon tears account for over 50% of sporting injuries [81], and can lead to chronic impairments [3]. Instrument assisted soft tissue mobilization (IASTM) is a manual therapy technique frequently used in the fields of sports rehabilitation and athletic training [82]. Clinical studies have shown IASTM improves outcomes for individuals with shoulder and patellar tendinopathy [35,37], and chronic ankle pain [38]. In animal studies, IASTM has been shown to increase fibroblast proliferation [40,41] and accelerate the rate of functional restoration during healing [27]. Several IASTM techniques are currently practiced [83], and while each technique has minor differences in tools and treatment protocols, they all involve the manual application of dynamic compressive loads by cyclic stroking of the damaged tissue through the skin with an instrument. Notably, none of the prevalent IASTM techniques specify the loading parameters that are recommended during treatment, yet experiments using tissue analogs have demonstrated the mechanosensitivity of cells to the magnitude and strain-rate of applied forces [52,75]. Therefore, in order to identify IASTM loading parameters that result in optimal patient outcomes, it is important to develop devices that can accurately apply IASTM to targeted forces and stroke frequencies.

Current techniques to evaluate IASTM in a research setting include instrumented hand-held devices and robotic manipulators. Hand-held devices are practical, but have not yet been validated to apply targeted loads and stroke frequencies [27,41,42,68–70,84]. Robotic manipulators can apply targeted loads and stroke frequencies [71,72], but these devices are stationary, expensive, and time intensive to operate, making them less practical for animal and human studies. The objective of this study was to develop a portable hand-held device that would enable users to accurately apply targeted forces and stroke frequencies during IASTM treatments.

4.2 Methods

4.2.1 Device Construction

A portable device (Figure. 19A) was constructed with a custom machined aluminum tip, uniaxial force sensor (Omegadyne, Sunbury, OH; 10N), stainless steel shaft, data acquisition module (National Instruments, Austin TX, USA; cDAQ-9171 & NI9237), and a tablet computer. The aluminum tip has a beveled edge similar to clinical IASTM tools (Figure 19B). Device operators will first input the targeted treatment

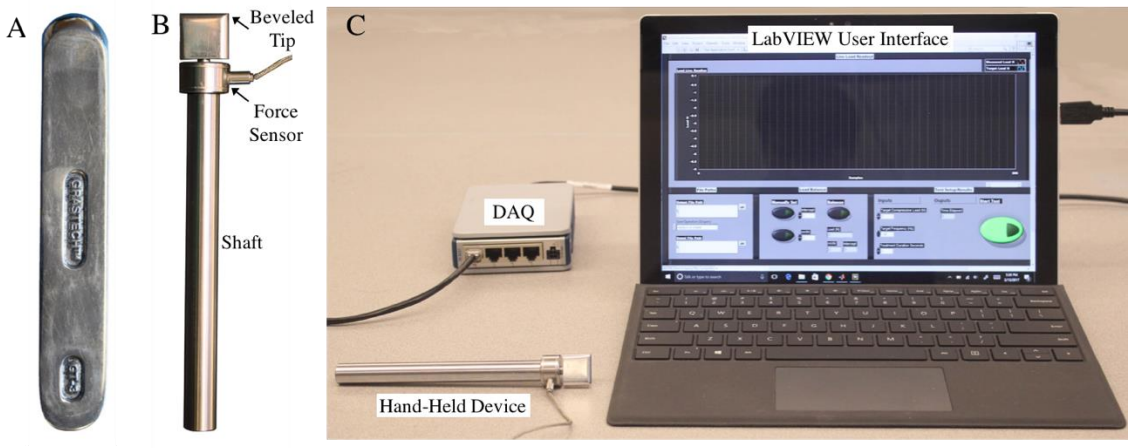

Figure 19: IASTM device design and components (A) Device components (B) Graston tool (C) Data acquisition and graphical user interface used with the device.

duration, peak compressive force, and stroke frequency into a custom LabVIEW program (Figure. 19C). The program then provides the operator feedback by displaying a live waveform of the applied load overlaid with a square waveform that shows the targeted loading profile. In

addition, the program creates an auditory signal that indicates when to start and end a stroke, acting as a metronome to guide stroke frequency. Peak compressive force was calculated by averaging all the force values measured during contact, where contact was defined using an automated graded threshold algorithm to identify clustered regions of data points (Figure. 20A). Stroke frequency was calculated by using a Fourier series summation [80] to fit the raw force measurement data with a non-linear least squares fitting method (Figure. 20B). The data acquisition software is free to download (*http://coen.boisestate.edu/ntm/software*).

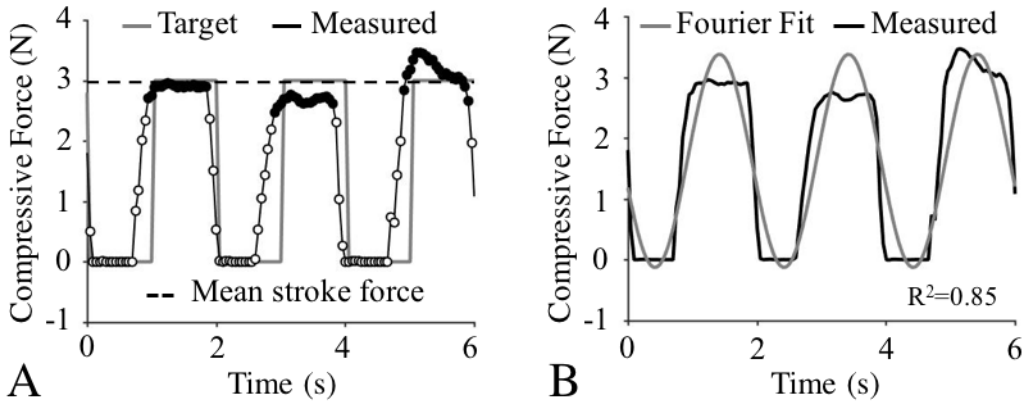

Figure 20: Automated calculation of loading parameters. (A) Load data measured by the device during performance testing overlaid with the target loading profile. Black circles represent data included in the calculation of mean stroke force, while open circles were excluded from this calculation. (B) Fourier series fit for measured load data with target frequency of 0.5Hz. Note: the compressive load is applied every half cycle.

4.2.2 Device Performance Tests

Two tests were executed to evaluate device accuracy. The first test analyzed the

device's accuracy in measuring compressive load when varying the angle between the device's shaft and the surface being treated (i.e. shaft angle). This test was performed using fixtures to anchor the device at five fixed angles between 50-90° (Figure 21A). At each fixed angle, the device was manually loaded three times from 0-5N, while the force normal to the surface was simultaneously measured with an auxiliary force sensor (Instron, Norwood, MA, USA; 1kN; Figure 21A). Data was collected for three minutes. The second test determined the device's accuracy in applying loads and stroke frequencies over a range of targeted values. This test was performed by having three individuals dynamically load a rigid foam block at eight different targeted loads (0.1-5N) and three different targeted frequencies (0.25, 0.5, 1.0 Hz). Each test was performed for

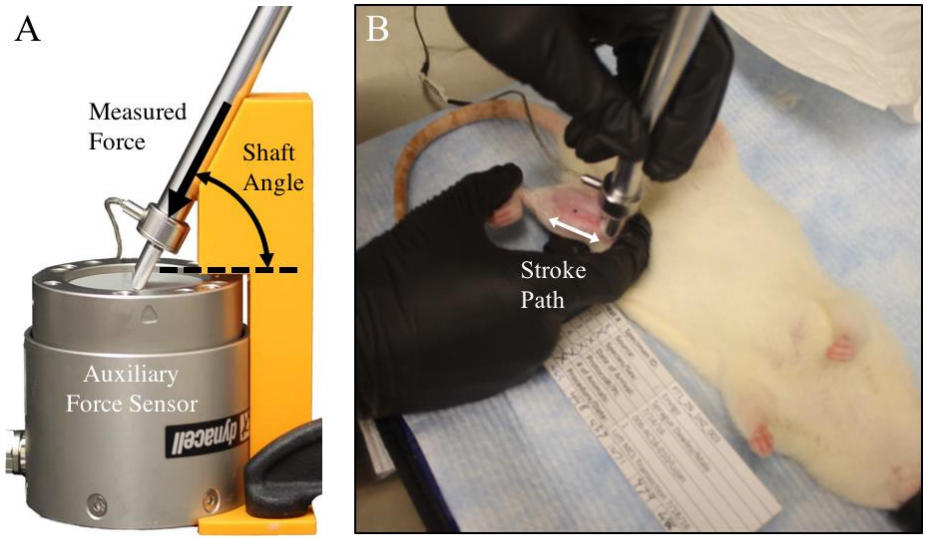

Figure 21: Experimental setup. A) Device at a 60 deg shaft angle to determine error between the force measured by the device and the compressive load applied to a surface, which is measured by an auxiliary force sensor. B) Device in use during the rodent experiment

one minute, and every test condition was performed three times by each operator. Each operator was allowed 30 minutes to practice using the device. In addition, a 1-minute practice run was performed prior to each test condition.

4.2.3 Experimental Validation

In order to test the repeatability of the device in a research setting, a pilot study was conducted utilizing three Sprague-Dawley rats (age = 6 months). The device was used to perform IASTM to medial collateral ligaments (MCL) that were injured through surgical transection. A 2N force was applied along the length of the MCL, between the tibial and femoral insertion, at a rate of 1 Hz for 1-minute (Figure 21B). These IASTM treatments were repeated 5x times during a 3-week period, and were based on guidelines for the Graston technique [34]. All procedures were approved by the Institutional Animal Care and Use Committee of Boise State University (# 006-AC16-01).

4.2.4 Statistical Tests

The effect of shaft angle on the device's accuracy in measuring compressive load was analyzed using linear regression. The effect of force magnitude, stroke frequency, and operator on the device's accuracy in applying the targeted loading parameters were assessed using a MANOVA, with LSD post hoc analysis. The effect of treatment time on the measured loading parameters during the animal experiment was assessed using repeated measures ANOVA. For all statistical tests, significance was set at $p<0.05$

4.3 Results

4.3.1 Device Performance Tests

For device shaft angles between 70°-90°, the device measurement error was less than 5%. Below 70° shaft angles, the device measurement error was greater than 15% (Figure 22A). Force was applied with less than 10% error for target magnitudes of 0.3 - 5.0N. For forces below 0.3N, the error was greater than 15% (Figure 22B). The average standard deviation in percent error during each one-minute test dropped from 28% to

12% as load increased from 0.3 to 5.0N. There was no impact of stroke frequency on the percent error in applied force across all force magnitudes (p=0.94). The stroke frequency was accurately applied with less than 0.2% error for all target values (Table 4). Error decreased with increasing frequencies (Table 1; p=0.02). Additionally, changing operators had no effect on device accuracy (p=0.94).

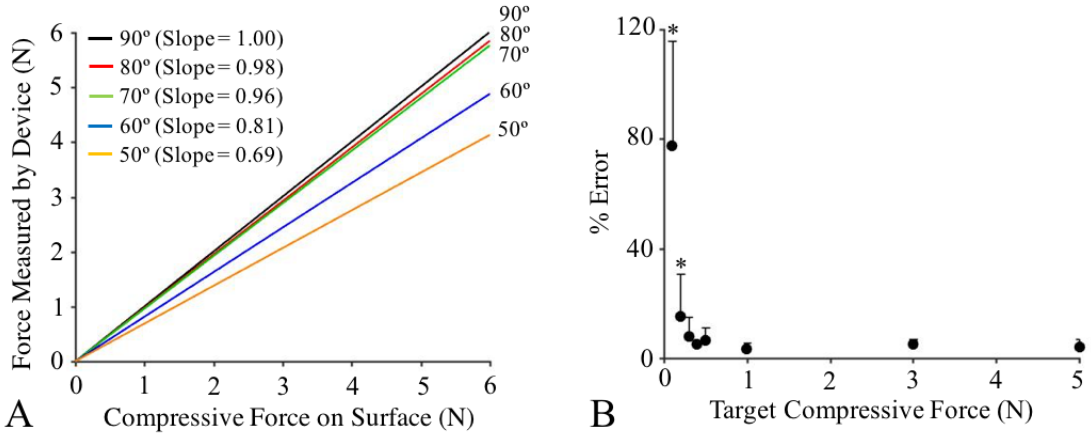

Figure 22: Results from device performance tests. (A) Comparison between the compressive force measured by the device and the compressive surface force measured by the auxiliary force sensor. A slope of 1 indicates the load measured by the device equals the compressive force applied to the surface. (B) Percent error in mean applied load at each targeted magnitude, averaged for three different operators. * = significantly different from all other targeted forces.

Table 4: Average stroke frequency across all tested loads (0.1-5.0N). The R^2 values are for the Fourier series summation fit of the measured load data.

Target Frequency (Hz)	Measured Frequency (Hz)	Error (%)	R^2
0.25	0.25 ± 0.01	0.13 ± 0.30	0.69 ± 0.14
0.50	0.50 ± 0.01	0.09 ± 0.13	0.69 ± 0.16
1.00	1.00 ± 0.01	0.04 ± 0.10	0.67 ± 0.14

4.3.2 Experimental Validation

The average percent error in load and stroke frequency across IASTM treatments was 4.5 ± 2.3% and 0.1 ± 0.1% respectively (Figure 23A). Additionally, there was no

effect of time of treatment on device accuracy (p=0.32) (Figure 23B). At a 95% confidence interval, values for mean load across all treatments ranged between 2.0 and 2.4 N. Therefore, there is 95% confidence that time of treatment and test subject had <10% effect on the mean load.

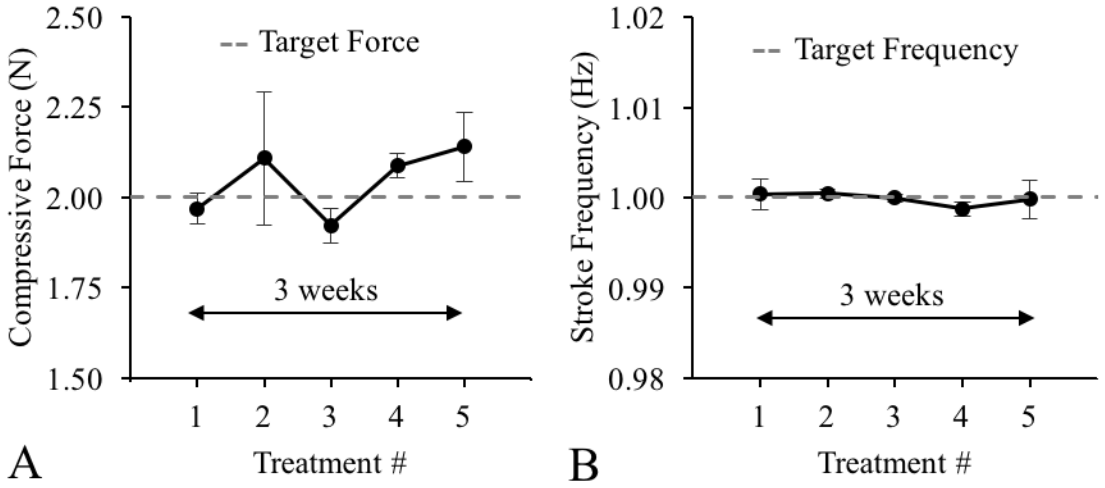

Figure 23: Results from experimental validation. (A) Average applied force and (B) average applied stroke frequency across five IASTM treatments for three rats.

4.4 Discussion

This study developed a hand-held device that can accurately apply targeted forces and stroke frequencies during IASTM treatments. Important guidelines for use include: 1) using shaft angles greater than 70°, where the device measurement error is less than 4%; and 2) applying targeted loads with compressive force between 0.3N–0.5N, where the error in applying a targeted load is less than 10%. Additionally, stroke frequencies of 1 Hz or less can be targeted with less than 1% error. By designing a simple and intuitive device, this level of accuracy was achieved for new operators with only 30 minutes of practice. To assist the quick adoption of this device by scientists and clinicians, the data acquisition software that provides visual and audio feedback to operators is freely

available to download (*http://coen.boisestate.edu/ntm/software*).

To our knowledge, this is the first hand-held device that has been validated to apply IASTM at targeted force magnitudes and stroke frequencies. Furthermore, this is the first study to demonstrate that these loading parameters can be repeatedly applied at multiple time points during *in vivo* animal experiments (Figure 23). Several researchers have prescribed forces during soft tissue mobilization through various techniques [40–42,68,84]; however, none of these methods were validated to apply a targeted force or stroke frequency. A drawback of our hand-held device is that although a mean load could be accurately applied, the coefficient of variation during each test was 12-28% of the applied load (Figure 22B). Previous robotic manipulators have 5% less variation [69], but disadvantages of robotic manipulators include less flexibility in the applied stroke path and a greater setup time, which may preclude the testing of large sample sizes.

This study has limitations. First, while the load range for the device is appropriate for many in-vivo research studies [40,41,52] and clinical studies of small joints [28], groups that want to apply loads greater than 10N would need to insert a different force sensor and conduct performance tests to determine device accuracy at higher force thresholds. Second, the hand-held device only measures normal force and would require a tri-axial force sensor to capture both normal and transverse force components [68]. However, this would increase device complexity and cost. Finally, while the sample size for the rat pilot study can estimate the device's error in applying targeted loading parameters across multiple weeks of treatment (Figure 23), future studies would require larger sample sizes to measure the dose-effect of targeted IASTM treatments on the functional restoration of injured tissue.

In conclusion, a portable hand-held device was successfully developed to apply targeted loading magnitudes and stroke frequencies during IASTM treatments. This validated device can assist researchers investigating the effect of compressive force parameters (magnitude and rate) on wound healing, and can support the optimization of IASTM protocols to improve patient care.

CHAPTER FIVE: CONCLUSIONS

5.1 Summary

The goal of this research was to develop in-vitro and in-vivo devices to determine optimal mechanical loading parameters to speed and strengthen healing of injured ligament. The in-vivo device is a hand-held device to control the frequency and magnitude of applied force during IASTM treatments. The device was validated to apply forces between 0 – 5N at frequencies from 0 – 1Hz with a high degree of accuracy and repeatability. The in-vitro device is a novel multi-axis mechanical stimulation bioreactor that can accurately apply tensile and combined tensile/compressive stress states to 3D fibroblast seeded tissue constructs. The bioreactor was validated to simultaneously apply cyclic forces from 0 – 0.2N with an accuracy of approximately 0.01N with a high degree of repeatability.

5.2 Future Work

5.2.1 In -Vivo Device

The IASTM tool will be used in more comprehensive experiments using the same rat model but with a larger sample size and a wider range of applied forces and stroke frequencies so that definitive effects of the stimulation can be observed.

5.2.2 In -Vitro Device

The bioreactor will be used in preliminary experiments on fibroblast seeded tissue constructs. However, prior to executing the experiment a robust tissue construct needs to be developed that can withstand mechanical stimulation without failure and has a

microstructure that can be manipulated by the fibroblast cells. Additionally, an efficient experimental design needs to be developed to maximize through-put from the single stimulation chamber.

Currently, a tissue construct created from collagen gel seeded with fibroblasts is being tested. The gels are seeded with NIH/3T3 mouse embryonic fibroblasts (ATCC, Manassas, VA) in to the collagen gel scaffold at 8.3 x 10^5 cells mL. The collagen scaffold has a collagen density of 1.45 mg/mL. The gels are created in dog bone shapes by casting them in custom molds (Figure 24A). The molds were machined from PTFE with a gauge width of 7 mm and gauge length of 21 mm (3:1 aspect ratio). Natural fiber pads (3M, St. Paul, MN) are placed in the ends of the mold to serve as mechanical constraints against cell driven contraction and to be used as a gripping surface in the bioreactor after the gels are removed from the molds (Figure 24B).

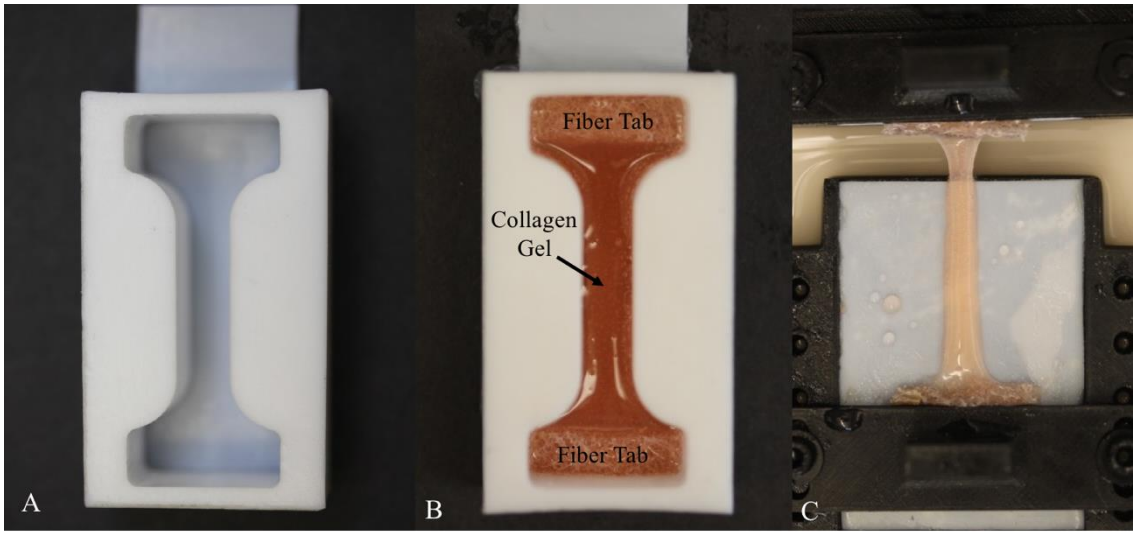

Figure 24: PTFE molds for collagen gel culture. (A) Empty mold (B) Mold with a cultured fibroblast seeded collagen gel (C) Collagen gel clamped in the bioreactor

The current proposed experimental design would include two groups. The first group would be a control group of non-stimulated gels that would remain in their

respective molds for 14 days. The second group would be a mechanically stimulated group. The gels would be allowed 3 days to culture statically to become strong enough to tolerate mechanical stimulation. The gels would then be loaded in the bioreactor for mechanical stimulation for the remaining 11 days. The sample would only be loaded in

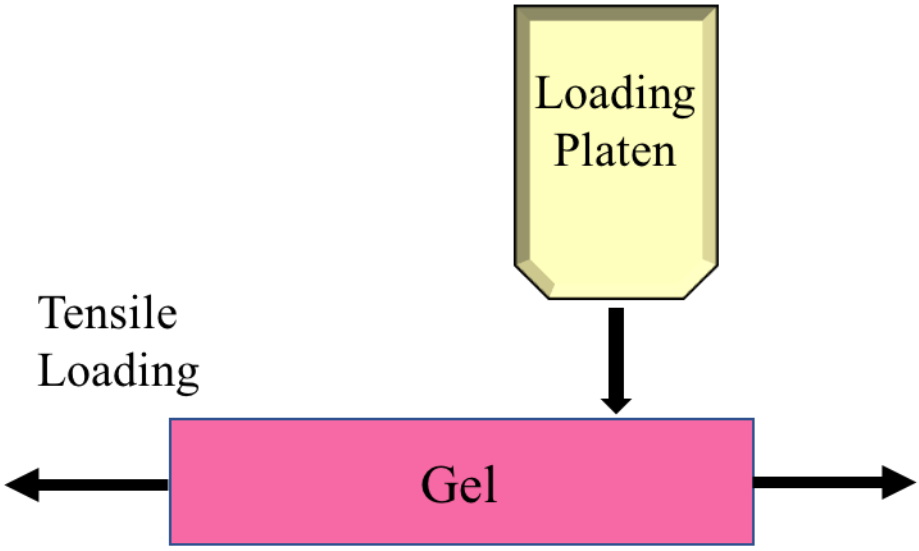

Figure 25: Proposed force controlled stimulation loading configuration. The loading platen only applies a compression to one half of the sample while the other half only received a tensile load. This allows the comparison of the effect of both loading conditions in one sample

tension and compression in one portion of the gel (Figure 25). After 14 days the samples will be mechanically tested in uniaxial tension to determine the elastic modulus of the tissue. The strain during the tensile test will be tracked through digital image correlation. The strain maps produce during the tensile tests are important because they will allow for the comparison of the stiffness of different regions of the gel. If the portion of the gel stimulated with combined loading has different strain behavior than the section loaded in only tension, then presumably there was some functional effect of the treatment.

REFERENCES

[1] Boden, B. P., Griffin, L. Y., and Garrett, W. E., 2000, "Etiology and Prevention of Noncontact ACL Injury.," Phys. Sportsmed., **28**(4), pp. 53–60.

[2] Chen, L. H., Warner, M., Fingerhut, L., and Makuc, D., 2009, "Injury Episodes and Circumstances: National Health Interview Survey, 1997-2007.," Vital Health Stat. 10., (241), pp. 1–55.

[3] van Rijn, R. M., van Os, A. G., Bernsen, R. M. D., Luijsterburg, P. a, Koes, B. W., and Bierma-Zeinstra, S. M. A., 2008, "What Is the Clinical Course of Acute Ankle Sprains? A Systematic Literature Review," Am. J. Med., **121**(4), p. 324–331.e7.

[4] Frank, C. B., Hart, D. A., and Shrive, N. G., 1999, "Molecular Biology and Biomechanics of Normal and Healing Ligaments - A Review," Osteoarthr. Cartil., **7**(1), pp. 130–140.

[5] Bischof, J. E., Spritzer, C. E., Caputo, A. M., Easley, M. E., DeOrio, J. K., Nunley, J. A., and DeFrate, L. E., 2010, "In Vivo Cartilage Contact Strains in Patients with Lateral Ankle Instability," J. Biomech., **43**(13), pp. 2561–2566.

[6] Shrive, N., Chimich, D., Marchuk, L., Wilson, J., Brant, R., and Frank, C., 1995, "Soft???tissue ???flaws??? Are Associated with the Material Properties of the Healing Rabbit Medial Collateral Ligament," J. Orthop. Res., **13**(6), pp. 923–929.

[7] Wang, J. H. C., and Thampatty, B. P., 2006, "An Introductory Review of Cell Mechanobiology," Biomech. Model. Mechanobiol., **5**(1), pp. 1–16.

[8] Woo, S. L., Gomez, M. a, Sites, T. J., Newton, P. O., Orlando, C. a, and Akeson, W. H., 1987, "The Biomechanical and Morphological Changes in the Medial Collateral Ligament of the Rabbit after Immobilization and Remobilization," J Bone Jt. Surg Am, **69**(8), pp. 1200–1211.

[9] Hart, D. P., and Dahners, L. E., 1987, "Healing of the Medial Collateral Ligament in Rats. The Effects of Repair, Motion, and Secondary Stabilizing Ligaments.," J. Bone Joint Surg. Am., **69**(8), pp. 1194–9.

[10] Benhardt, H. A., and Cosgriff-Hernandez, E. M., 2009, "The Role of Mechanical

Loading in Ligament Tissue Engineering," Tissue Eng. Part B Rev., **15**(4), pp. 467–475.

[11] Mauck, R. L., Soltz, M. a, Wang, C. C., Wong, D. D., Chao, P. H., Valhmu, W. B., Hung, C. T., and Ateshian, G. a, 2000, "Functional Tissue Engineering of Articular Cartilage through Dynamic Loading of Chondrocyte-Seeded Agarose Gels.," J. Biomech. Eng., **122**(3), pp. 252–260.

[12] Frank, C. B., 2004, "Ligament Structure, Physiology and Function," J. Musculoskelet. Neuronal Interact., **4**(2), pp. 199–201.

[13] Hauser, R. a, Dolan, E. E., Phillips, H. J., Newlin, a C., Moore, R. E., and Woldin, B. a, 2013, "Ligament Injury and Healing: A Review of Current Clinical Diagnostics and Therapeutics," Open Rehabil. J., **6**(May 2014), pp. 1–20.

[14] Wenger, K. H., El-Awady, A. R., Messer, R. L. W., Sharawy, M. M., White, G., and Lapp, C. A., 2011, "Pneumatic Pressure Bioreactor for Cyclic Hydrostatic Stress Application: Mechanobiology Effects on Periodontal Ligament Cells.," J. Appl. Physiol. (Bethesda, Md. 1985), **111**(4), pp. 1072–1079.

[15] Bates, N. A., Nesbitt, R. J., Shearn, J. T., Myer, G. D., and Hewett, T. E., 2015, "Relative Strain in the Anterior Cruciate Ligament and Medial Collateral Ligament During Simulated Jump Landing and Sidestep Cutting Tasks," Am. J. Sports Med., **43**(9), pp. 2259–2269.

[16] Lujan, T. J., Dalton, M. S., Thompson, B. M., Ellis, B. J., and Weiss, J. a, 2007, "Effect of ACL Deficiency on MCL Strains and Joint Kinematics.," J. Biomech. Eng., **129**(3), pp. 386–392.

[17] Mancini, E. J., Kohen, R., Esquivel, A. O., Cracchiolo, A. M., and Lemos, S. E., 2017, "Comparison of ACL Strain in the MCL-Deficient and MCL-Reconstructed Knee During Simulated Landing in a Cadaveric Model," Am. J. Sports Med., **45**(5), pp. 1090–1094.

[18] Hubbard, T. J., 2008, "Ligament Laxity Following Inversion Injury with and without Chronic Ankle Instability," Foot Ankle Int., **29**(3), pp. 305–311.

[19] Mirkin, G., and Hoffmain, M., 1978, *The Sportsmedicine Book.*

[20] Van Den Bekerom, M. P. J., Struijs, P. A. A., Blankevoort, L., Welling, L., Van Welling, C. N., and Kerkhoffs, G. M. M. J., 2012, "What Is the Evidence for Rest, Ice, Compression, and Elevation Therapy in the Treatment of Ankle Sprains in Adults?," J. Athl. Train., **47**(4), pp. 435–443.

[21] Hoffmann, A., and Gross, G., 2006, "Tendon and Ligament Engineering: From Cell Biology to in Vivo Application.," Regen. Med., **1**(4), pp. 563–74.

[22] Laurencin, C., Khan, Y., Kofron, M., El-Amin, S., Botchwey, E., Yu, X., and Cooper, J., 2006, "Tissue Engineering of Bone and Ligament: A 15-Year Perspective," Clin. Orthop. Res., **447**, pp. 221–236.

[23] Warden, S. J., Avin, K. G., Beck, E. M., DeWolf, M. E., Hagemeier, M. A., and Martin, K. M., 2006, "Low-Intensity Pulsed Ultrasound Accelerates and a Nonsteroidal Anti-Inflammatory Drug Delays Knee Ligament Healing," Am. J. Sports Med., **34**(7), pp. 1094–1102.

[24] van Os, A. G., Bierma-Zeinstra, S. M. a, Verhagen, A. P., de Bie, R. a, Luijsterburg, P. a J., and Koes, B. W., 2005, "Comparison of Conventional Treatment and Supervised Rehabilitation for Treatment of Acute Lateral Ankle Sprains: A Systematic Review of the Literature.," Jospt, **35**(2), pp. 95–105.

[25] Lin, C.-W. C., Hiller, C. E., and de Bie, R. A., 2010, "Evidence-Based Treatment for Ankle Injuries: A Clinical Perspective," J. Man. Manip. Ther., **18**(1), pp. 22–28.

[26] Barnes, P. M., Bloom, B., and Nahin, R. L., 2008, "Complementary and Alternative Medicine Use among Adults and Children: United States, 2007.," Natl. Health Stat. Report., (12), pp. 1–23.

[27] Loghmani, M. T., and Warden, S. J., 2009, "Instrument-Assisted Cross-Fiber Massage Accelerates Knee Ligament Healing," J Orthop Sport. Phys Ther, **39**(7), pp. 506–514.

[28] Terry Loghmani, M., Bayliss, A. J., Clayton, G., and Gundeck, E., 2015, "Successful Treatment of a Guitarist with a Finger Joint Injury Using Instrument-Assisted Soft Tissue Mobilization: A Case Report.," J. Man. Manip. Ther., **23**(5),

pp. 246–53.

[29] Hammer, W. I., 2008, “The Effect of Mechanical Load on Degenerated Soft Tissue,” J. Bodyw. Mov. Ther., **12**(3), pp. 246–256.

[30] Nielsen, A., Knoblauch, N. T. M., Dobos, G. J., Michalsen, A., and Kaptchuk, T. J., 2007, “The Effect of Gua Sha Treatment on the Microcirculation of Surface Tissue: A Pilot Study in Healthy Subjects,” Explor. J. Sci. Heal., **3**(5), pp. 456–466.

[31] Kivlan, B. R., Carcia, C. R., Clemente, F. R., Phelps, A. L., and Martin, R. L., 2015, “The Effect of Astym® Therapy on Muscle Strength: A Blinded, Randomized, Clinically Controlled Trial,” BMC Musculoskelet. Disord., **16**(1), p. 325.

[32] Markovic, G., 2015, “Acute Effects of Instrument Assisted Soft Tissue Mobilization vs. Foam Rolling on Knee and Hip Range of Motion in Soccer Players,” J. Bodyw. Mov. Ther., **19**(4), pp. 690–696.

[33] Hayes D, Loghmani MT, Lubitz R, M. E., 2007, “A Comparison of 2 Instru-Ment-Assisted Soft Tissue Mobilization Techniques: Effects on Therapist Discomfort/fatigue and Treatment Time [Abstract],” Orthop Sport. Phys Ther, **37**(Abstract No. OPL19.).

[34] Hyde, T. E., and Gengenbach, M. S., 2007, *Conservative Management of Sports Injuries*, Jones & Bartlett Learning, Sudbury, MA.

[35] Aspegren, D., Hyde, T., and Miller, M., 2007, “Conservative Treatment of a Female Collegiate Volleyball Player with Costochondritis,” J Manip. Physiol Ther, **30**(4), pp. 321–325.

[36] Miners, A. L., and Bougie, T. L., 2011, “Chronic Achilles Tendinopathy: A Case Study of Treatment Incorporating Active and Passive Tissue Warm-Up, Graston Technique, ART, Eccentric Exercise, and Cryotherapy,” J Can Chiropr Assoc, **55**(4), pp. 269–279.

[37] Wilson, J., Sevier, T., Helfst, R., Honing, E., and Thomann, A., 2000, “Comparison of Rehabilitation Methods in the Treatment of Patellar Tendinitis.,”

J. Sport. Rehabil., **9**(4), pp. 301–314.

[38] Melham, T. J., Sevier, T. L., Malnofski, M. J., Wilson, J. K., and Helfst, R. H., 1998, "Chronic Ankle Pain and Fibrosis Successfully Treated with a New Noninvasive Augmented Soft Tissue Mobilization Technique (ASTM): A Case Report.," Med. Sci. Sports Exerc., **30**(6), pp. 801–4.

[39] Howitt, S., Jung, S., and Hammonds, N., 2009, "Conservative Treatment of a Tibialis Posterior Strain in a Novice Triathlete: A Case Report.," J. Can. Chiropr. Assoc., **53**(1), pp. 23–31.

[40] Davidson, C. J., Ganion, L. R., Gehlsen, G. M., Verhoestra, B., Roepke, J. E., and Sevier, T. L., 1997, "Rat Tendon Morphologic and Functional Changes Resulting from Soft Tissue Mobilization," Med Sci Sport. Exerc, **29**(3), pp. 313–319.

[41] Gehlsen, G. M., Ganion, L. R., and Helfst, R., 1999, "Fibroblast Responses to Variation in Soft Tissue Mobilization Pressure.," Med. Sci. Sports Exerc., **31**(4), pp. 531–5.

[42] Loghmani, M. T., Neff, B., Alotaibi, A. M., Anwar, S., Chien, S., and March, K., 2016, "Quantifiable Soft Tissue Manipulation (QSTM): A Requisite to Advance the Field of Manual Therapy," pp. 6–8.

[43] Mills, S., Cowin, A., and Kaur, P., 2013, "Pericytes, Mesenchymal Stem Cells and the Wound Healing Process," Cells, **2**(3), pp. 621–634.

[44] Gauglitz, G., and Korting, H., 2011, "Hypertrophic Scarring and Keloids: Pathomechanisms and Current and Emerging Treatment Strategies," Mol. Med., **17**(1–2), p. 1.

[45] Loghmani, M. T., and Warden, S. J., 2013, "Instrument-Assisted Cross Fiber Massage Increases Tissue Perfusion and Alters Microvascular Morphology in the Vicinity of Healing Knee Ligaments.," BMC Complement. Altern. Med., **13**(1).

[46] Molloy, T., Wang, Y., and Murrell, G. A. C., 2003, "The Roles of Growth Factors in Tendon and Ligament Healing," Sport. Med., **33**(5), pp. 381–394.

[47] Vardiman, J. P., Siedlik, J., Herda, T., Hawkins, W., Cooper, M., Graham, Z. A.,

Deckert, J., Gallagher, P., Science, E., States, U., Science, B., and City, K., 2015, “Instrument-Assisted Soft Tissue Mobilization : E Ff Ects on the Properties of Human Plantar Flexors,” Int. J. Sports Med., **36**(3), pp. 197–203.

[48] Nettelhoff, L., Grimm, S., Jacobs, C., Walter, C., Pabst, A. M., Goldschmitt, J., and Wehrbein, H., 2016, “Influence of Mechanical Compression on Human Periodontal Ligament Fibroblasts and Osteoblasts,” Clin. Oral Investig., **20**(3), pp. 621–629.

[49] Balestrini, J. L., and Billiar, K. L., 2009, “Magnitude and Duration of Stretch Modulate Fibroblast Remodeling.,” J. Biomech. Eng., **131**(5), p. 51005.

[50] Balestrini, J. L., and Billiar, K. L., 2006, “Equibiaxial Cyclic Stretch Stimulates Fibroblasts to Rapidly Remodel Fibrin,” J. Biomech., **39**(16), pp. 2983–2990.

[51] Berry, C. C., Shelton, J. C., Bader, D. L., and Lee, D. A., 2003, “Influence of External Uniaxial Cyclic Strain on Oriented Fibroblast-Seeded Collagen Gels.,” Tissue Eng., **9**(4), pp. 613–24.

[52] Joshi, S. D., and Webb, K., 2008, “Variation of Cyclic Strain Parameters Regulates Development of Elastic Modulus in Fibroblast/substrate Constructs,” J. Orthop. Res., **26**(8), pp. 1105–1113.

[53] Martínez, H., Brackmann, C., Enejder, A., and Gatenholm, P., 2012, “Mechanical Stimulation of Fibroblasts in Micro-Channeled Bacterial Cellulose Scaffolds Enhances Production of Oriented Collagen Fibers,” J. Biomed. Mater. Res. - Part A, **100 A**(4), pp. 948–957.

[54] Chen, C. S., 2008, “Mechanotransduction - a Field Pulling Together?,” J. Cell Sci., **121**(20), pp. 3285–3292.

[55] Muhamed, I., Chowdhury, F., and Maruthamuthu, V., 2017, “Biophysical Tools to Study Cellular Mechanotransduction,” Bioengineering, **4**(1), p. 12.

[56] Hattner, R. S., 1968, “‘Influence of Weightlessness upon the Skeleton: A Review.’.,” Aerosp. Med., **0001**–**9402,**(8), p. 849.

[57] Duval, K., Grover, H., Han, L.-H., Mou, Y., Pegoraro, A. F., Fredberg, J., and

Chen, Z., 2017, “Modeling Physiological Events in 2D vs. 3D Cell Culture,” Physiology, **32**(4), pp. 266–277.

[58] Gentleman, E., Livesay, G. A., Dee, K. C., and Nauman, E. A., 2006, “Development of Ligament-Like Structural Organization and Properties in Cell-Seeded Collagen Scaffolds in Vitro,” Ann. Biomed. Eng., **34**(5), pp. 726–736.

[59] Thomopoulos, S., Fomovsky, G. M., and Holmes, J. W., 2005, “The Development of Structural and Mechanical Anisotropy in Fibroblast Populated Collagen Gels.,” J. Biomech. Eng., **127**(5), pp. 742–750.

[60] Juncosa-Melvin, N., Matlin, K. S., Holdcraft, R. W., Nirmalanandhan, V. S., and Butler, D. L., 2007, “Mechanical Stimulation Increases Collagen Type I and Collagen Type III Gene Expression of Stem Cell-Collagen Sponge Constructs for Patellar Tendon Repair.,” Tissue Eng., **13**(6), pp. 1219–1226.

[61] Brown, T. D., 2000, “Techniques for Mechanical Stimulation of Cells in Vitro: A Review,” J. Biomech., **33**(1), pp. 3–14.

[62] Bilgen, B., Chu, D., Stefani, R., and Aaron, R. K., 2013, “Design of a Biaxial Mechanical Loading Bioreactor for Tissue Engineering.,” J. Vis. Exp., (74), p. e50387.

[63] Wartella, K. a, and Wayne, J. S., 2009, “Bioreactor for Biaxial Mechanical Stimulation to Tissue Engineered Constructs,” J. Biomech. Eng., **131**(4), pp. 1–5.

[64] Wang, T., Gardiner, B. S., Lin, Z., Rubenson, J., Kirk, T. B., Wang, A., Xu, J., Smith, D. W., Lloyd, D. G., and Zheng, M. H., 2013, “Bioreactor Design for Tendon/Ligament Engineering.”

[65] Gehlsen, G. M., Ganion, L. R., and Helfst, R., 1999, “Fibroblast Responses to Variation in Soft Tissue Mobilization Pressure.,” Med. Sci. Sports Exerc., **31**(4), pp. 531–5.

[66] Weidenhamer, N. K., and Tranquillo, R. T., 2013, “Influence of Cyclic Mechanical Stretch and Tissue Constraints on Cellular and Collagen Alignment in Fibroblast-Derived Cell Sheets.,” Tissue Eng. Part C. Methods, **19**(5), pp. 386–95.

[67] Imai, K., Ikoma, K., Chen, Q., Zhao, C., An, K. N., and Gay, R. E., 2015, "Biomechanical and Histological Effects of Augmented Soft Tissue Mobilization Therapy on Achilles Tendinopathy in a Rabbit Model," J. Manipulative Physiol. Ther., **38**(2), pp. 112–118.

[68] Lee, H.-M., Wu, S.-K., and You, J.-Y., 2009, "Quantitative Application of Transverse Friction Massage and Its Neurological Effects on Flexor Carpi Radialis," Man. Ther., **14**(5), pp. 501–507.

[69] Zoest, G. G. J. M., van den Berg, H. T. C. M., and Holtkamp, F. C., 2002, "Three-Dimensionality of Contact Forces during Clinical Manual Examination and Treatment: A New Measuring System," Clin. Biomech., **17**(9–10), pp. 719–722.

[70] Neil Tuttle, 2011, "Design and Construction of a Novel Low-Cost Device to Provide Feedback on Manually Applied Forces," J. Orthop. Sport. Phys. Ther., **41**(3), pp. 174-A11.

[71] Wang, Q., Zeng, H., Best, T. M., Haas, C., Heffner, N. T., Agarwal, S., and Zhao, Y., 2014, "A Mechatronic System for Quantitative Application and Assessment of Massage-Like Actions in Small Animals," Ann. Biomed. Eng., **42**(1), pp. 36–49.

[72] Zeng, H., Butterfield, T. A., Agarwal, S., Haq, F., Best, T. M., and Zhao, Y., 2008, "An Engineering Approach for Quantitative Analysis of the Lengthwise Strokes in Massage Therapies," J. Med. Device., **2**(4), pp. 41003–41008.

[73] Zeichen, J., van Griensven, M., and Bosch, U., 2000, "The Proliferative Response of Isolated Human Tendon Fibroblasts to Cyclic Biaxial Mechanical Strain.," Am. J. Sports Med., **28**(6), pp. 888–892.

[74] Papadopoulou, A., Iliadi, A., Eliades, T., and Kletsas, D., 2016, "Early Responses of Human Periodontal Ligament Fibroblasts to Cyclic and Static Mechanical Stretching.," Eur. J. Orthod., (5), pp. 1–6.

[75] Nirmalanandhan, V. S., Shearn, J. T., Juncosa-Melvin, N., Rao, M., Gooch, C., Jain, A., Bradica, G., and Butler, D. L., 2008, "Improving Linear Stiffness of the Cell-Seeded Collagen Sponge Constructs by Varying the Components of the Mechanical Stimulus," Tissue Eng. Part A, **14**(11), pp. 1883–1891.

[76] Budynas, R., and Nisbett, J., 2015, *Shigley's Mechanical Engineering Design, Tenth Edition*.

[77] Steinwachs, J., Metzner, C., Skodzek, K., Lang, N., Thievessen, I., Mark, C., Münster, S., Aifantis, K. E., and Fabry, B., 2016, "Three-Dimensional Force Microscopy of Cells in Biopolymer Networks.," Nat. Methods, **13**(2), pp. 171–176.

[78] Roeder, B. A., Kokini, K., and Voytik-Harbin, S. L., 2009, "Fibril Microstructure Affects Strain Transmission within Collagen Extracellular Matrices.," J. Biomech. Eng., **131**(3), p. 31004.

[79] Han, W. M., Heo, S. J., Driscoll, T. P., Smith, L. J., Mauck, R. L., and Elliott, D. M., 2013, "Macro- to Microscale Strain Transfer in Fibrous Tissues Is Heterogeneous and Tissue-Specific," Biophys. J., **105**(3), pp. 807–817.

[80] 2017, "Fourier Series," MathWorks [Online]. Available: https://www.mathworks.com/help/curvefit/fourier.html.

[81] Fernandez, W. G., Yard, E. E., and Comstock, R. D., 2007, "Epidemiology of Lower Extremity Injuries among U.S. High School Athletes," Acad. Emerg. Med., **14**(7), pp. 641–645.

[82] Kim, J., Sung, D. J., and Lee, J., 2017, "Therapeutic Effectiveness of Instrument-Assisted Soft Tissue Mobilization for Soft Tissue Injury : Mechanisms and Practical Application," J. Exerc. Rehabil., **13**(1), pp. 12–22.

[83] Cheatham, S. W., Lee, M., Cain, M., and Baker, R., 2016, "The Efficacy of Instrument Assisted Soft Tissue Mobilization: A Systematic Review," J Can Chiropr Assoc, **60**(3), pp. 200–211.

[84] Imai, K., Ikoma, K., Chen, Q., Zhao, C., An, K. N., and Gay, R. E., 2015, "Biomechanical and Histological Effects of Augmented Soft Tissue Mobilization Therapy on Achilles Tendinopathy in a Rabbit Model," J. Manipulative Physiol. Ther., **38**(2), pp. 112–118.

[85] 2017, "Common Conditions," Fultch Pod. [Online]. Available: http://futchpodiatry.com/common-conditions/.

[86] Ohland, K. J., Woo, S. L.-Y., Weiss, J. A., Takai, S., and Shelley, F. J., 1991, "Healing of Combined Injuries of the Rabbit Medial Collateral Ligament and Its Insertions: A Long Term Study on the Effects of Conservative vs. Surgical Treatment.," Proc. Winter Annu. Meet. Am. Soc. Mech. Eng. Atlanta, GA.

[87] 2017, "Graston Technique," O.S.R. Phys. Ther. [Online]. Available: https://www.osrpt.com/physical-therapy/graston-technique/.